Check for updates

Geochemistry, Geophysics, Geosystems®

AGU ADVANCING EARTH AND SPACE SCIENCE

RESEARCH ARTICLE
10.1029/2022GC010670

Key Points:
- A major pulse of 25–22 Ma volcanism is documented on the Loyalty and Three Kings Ridges, southwest Pacific Ocean
- The ridges are part of a more than 3,000 km long belt of Eocene to Miocene remnant volcanic arcs, stranded along the edge of Zealandia
- With care in sample selection, and petrological work, meaningful Ar/Ar ages can be obtained from altered and/or very low-K submarine basalts

Correspondence to:
N. Mortimer,
n.mortimer@gns.cri.nz

Detailed ^{40}Ar/^{39}Ar Geochronology of the Loyalty and Three Kings Ridges Clarifies the Extent and Sequential Development of Eocene to Miocene Southwest Pacific Remnant Volcanic Arcs

P. B. Gans[1], N. Mortimer[2], M. Patriat[3], R. E. Turnbull[2], M. P. Crundwell[4], A. Agranier[3], A. T. Calvert[5], G. Seward[1], S. Etienne[6], P. M. J. Durance[4], H. J. Campbell[4], and J. Collot[6]

[1]University of California, Santa Barbara, CA, USA, [2]GNS Science, Dunedin, New Zealand, [3]CNRS, Ifremer, Geo-Ocean, University of Brest, Plouzané, France, [4]GNS Science, Lower Hutt, New Zealand, [5]U.S. Geological Survey, Menlo Park, CA, USA, [6]Service Géologique de Nouvelle Calédonie, Nouméa, New Caledonia

Abstract The 2015 VESPA voyage (Volcanic Evolution of South Pacific Arcs) was a seismic and rock dredging expedition to the Loyalty and Three Kings Ridges and South Fiji Basin. In this paper we present 33 ^{40}Ar/^{39}Ar, 22 micropaleontological, and two U/Pb ages for igneous and sedimentary rocks from 33 dredge sites in this little-studied part of the southwest Pacific Ocean. Igneous rocks include basalts, dolerites, basaltic andesites, trachyandesites, and a granite. Successful Ar/Ar dating of altered and/or low-K basalts was achieved through careful sample selection and processing, detailed petrographic and element mapping of groundmass, and incremental heating experiments on both phenocryst and groundmass separates to interpret the complex spectra produced by samples having multiple K reservoirs. The ^{40}Ar/^{39}Ar ages of most of the sampled lavas, irrespective of composition, are latest Oligocene to earliest Miocene (25–22 Ma); two are Eocene (39–36 Ma). The granite has a U/Pb zircon age of 23.6 ± 0.3 Ma. ^{40}Ar/^{39}Ar lava ages are corroborated by microfossil ages from associated sedimentary rocks. The VESPA lavas are part of a >3,000 km long disrupted belt of Eocene to Miocene subduction-related volcanic rocks. The belt includes arc rocks in Northland New Zealand, Northland Plateau, Three Kings Ridge, and Loyalty Ridge and, speculatively, D'Entrecasteaux Ridge. This belt is the product of superimposed Eocene and Oligocene-Miocene remnant volcanic arcs that were stranded along and near the edge of Zealandia while still-active arc belts migrated east with the Pacific trench.

Plain Language Summary Samples of lava from the seabed between New Zealand and New Caledonia have been dated using atomic clocks and fossils. Most lavas erupted in a big pulse of volcanic activity between 25 and 22 million years ago. They are part of a belt of now-extinct undersea volcanoes that stretches for more than 3,000 km between New Zealand and the Solomon Islands. These volcanoes were formed by subduction of the Pacific Plate under the Australian Plate.

1. Introduction

Subduction, volcanic arcs, and back-arc basins are integral components of the plate tectonics paradigm. Since the pioneering work of Karig (1971), the western and southwestern parts of the Pacific Ocean have been recognized as the main areas on Earth where arrays of little-modified remnant arcs and back-arc basins are preserved behind currently active systems (Figure 1, e.g., Gurnis et al., 2004; Hall, 2002; Taylor & Karner, 1983). In both areas, events and processes associated with the Pliocene-active magmatic arcs and their back-arc basins are well-studied for example, Izu-Bonin arc and basins, and Tonga-Kermadec arc and Lau Basin (e.g., Gill et al., 2021; Stern et al., 2003). In contrast, the earlier, Eocene-Miocene rocks west of the active arcs in these regions have received less attention although this is changing for the western Pacific (e.g., Ishizuka et al., 2011).

The remnant arcs and basins of the southwest Pacific offer an opportunity to explore processes of subduction initiation, arc longevity, arc-splitting, back-arc basin opening and subduction polarity switching. These processes feature prominently in many tectonic models of older Phanerozoic orogens, where evidence is often tenuous and heavily overprinted by later collisional/crustal shortening events. The mainly submarine nature of the southwest Pacific arcs and associated back-arc basins means, however, that they must be investigated by marine geophysical profiling, multibeam bathymetry, rock dredging, and rock drilling methods (e.g., Herzer et al., 2011; Mortimer et al., 2007; Sutherland et al., 2019). Determining reliable ages from the predominantly mafic volcanic rocks from marine expeditions is of critical importance to petrogenetic models and tectonic reconstructions. ^{40}Ar/^{39}Ar dating

Investigation: P. B. Gans, N. Mortimer, M. Patriat, R. E. Turnbull, M. P. Crundwell, A. Agranier, A. T. Calvert, G. Seward, S. Etienne, P. M. J. Durance, H. J. Campbell, J. Collot
Methodology: P. B. Gans, N. Mortimer, R. E. Turnbull, A. T. Calvert
Project Administration: N. Mortimer, M. Patriat
Resources: N. Mortimer, M. Patriat, R. E. Turnbull, P. M. J. Durance, J. Collot
Validation: N. Mortimer, M. Patriat, A. T. Calvert, H. J. Campbell, J. Collot
Visualization: N. Mortimer
Writing – original draft: P. B. Gans, N. Mortimer, M. Patriat
Writing – review & editing: P. B. Gans, N. Mortimer, M. Patriat, R. E. Turnbull, M. P. Crundwell, A. Agranier, A. T. Calvert, S. Etienne, P. M. J. Durance, H. J. Campbell, J. Collot

is one of the few suitable methods available. However, even this is commonly hampered by alteration and very low K contents of the sampled rocks.

Key research questions about the southwest Pacific arc and back-arc basin system include: (a) precisely where and when did Cenozoic subduction initiate? (b) what was the space-time relationship between arc magmatism and the opening of adjacent basins? (c) what were the driving forces for these magmatic and tectonic changes (i.e., Pacific trench rollback or subduction polarity reversals)? To help answer these questions, the 25-day VESPA (Volcanic Evolution of South Pacific Arcs) research voyage of N/O *l'Atalante* in 2015 undertook seismic reflection profiling and rock dredging of the Norfolk, Loyalty, and Three Kings Ridge area between New Zealand and New Caledonia (Figure 1; Mortimer & Patriat, 2016). Post-voyage analyses and interpretations provide much new information relevant to the Cenozoic magmatic and tectonic development of the region.

The main purpose of this paper is to present the results of a comprehensive new Ar/Ar geochronological investigation of dredge samples of submarine volcanic rocks collected during the VESPA voyage. The data comprise 49 individual $^{40}Ar/^{39}Ar$ phenocryst and groundmass ages from 33 separate samples of lava. The Ar/Ar ages are supplemented by U/Pb dating of zircons from a granite and a sandstone, and micropaleontological dating of 22 limestone and mudstone samples associated with the submarine lavas. An important outcome of this investigation is a better understanding of the argon systematics and complexities of very low-potassium and/or hydrothermally altered submarine volcanic rocks. By integrating detailed petrographic, microprobe, and argon incremental heating studies, we shed light on how potassium is distributed in different reservoirs in these types of samples and how this results in different $^{40}Ar/^{39}Ar$ age spectrum shapes. Consequently, we are able to recommend methodologies for sample preparation, analytical procedures, and interpretation of complex age spectra that are likely to yield optimum results. We use the dating results to define new age-composition patterns in southwest Pacific lavas. In turn, these can be used to test tectonic models of arc inception, longevity, and migration.

This paper builds on previously published results from the VESPA voyage (Lawrence et al., 2020; Mortimer et al., 2021; Patriat et al., 2018) as well as results from previous research cruises to the region (Ballance et al., 1999; Bernardel et al., 2002; Crawford, 2004; Herzer et al., 2011; Meffre et al., 2006; Mortimer et al., 1998, 2007, 2010, 2014, 2018; Seton et al., 2016; Sutherland et al., 2019). This is a companion paper to one that addresses the geochemistry and petrogenesis of VESPA lavas (Agranier et al., 2023).

2. Southwest Pacific Tectonic Framework

The two principal geotectonic features of the southwest Pacific are the 95% submerged continent of Te Riu-a-Māui/Zealandia and the Pacific-Australian plate boundary (Figure 1; Mortimer et al., 2017). A broad region of active and remnant volcanic arcs and back-arc basins lies east of Zealandia and across its northeastern margin. The active arcs and basins comprise the Taupō-Kermadec-Tonga and Vanuatu arcs, the Havre Trough and Lau and North Fiji Basins. The inactive features include the Colville-Lau, Three Kings, Loyalty, D'Entrecasteaux and Rennell Ridges and Vitiaz Trench Lineament, and the Norfolk, South Fiji, North Loyalty, D'Entrecasteaux, and Santa Cruz Basins. There is an along-strike change in the polarity of active subduction, with Pacific Plate dipping west under the Taupō-Tonga-Kermadec arc and Australian Plate dipping northeast under the Vanuatu arc.

The current cycle of southwest Pacific subduction-related tectonics is inferred to have started in the Eocene, or possibly the Late Cretaceous or Paleocene (e.g., Collot et al., 2020; Crawford et al., 2003; Schellart et al., 2006; Sutherland et al., 2017; Whattam, 2009; Whattam et al., 2008). Grande Terre of New Caledonia and the North Island of New Zealand provide onland exposures of the geology of Zealandia. In both onland areas, obducted ophiolitic nappes are present (Isaac et al., 1994; Maurizot, Robineau, et al., 2020). In New Zealand, a 500-km-long, 22–17 Ma subduction-related volcanic arc, the Northland Arc, erupted through and across the nappes (e.g., Hayward et al., 2001; Mortimer et al., 2010). In contrast, in onland New Caledonia post-obduction igneous activity is restricted to just two Oligocene granitoid stocks (Paquette & Cluzel, 2007; Sevin et al., 2020). Reconnaissance dredging and drilling has sampled scattered Eocene, Oligocene, and Miocene igneous rocks from the Rennell Ridge, D'Entrecasteaux Ridge and Basin, Norfolk Ridge and Basin, Three Kings Ridge, South Fiji Basin, and Northland Plateau (Mortimer et al., 1998, 2007, 2010, 2014, 2021). Most of these earlier sampling campaigns yielded predominantly latest Oligocene to early Miocene (24–19 Ma) ages. Until the VESPA voyage, the Loyalty Ridge was the only major southwest Pacific ridge not to have been sampled, despite its commonly cited interpretation as an Eocene volcanic arc (Crawford et al., 2003; Maurizot, Cluzel, et al., 2020; Schellart et al., 2006; Whattam, 2009; Whattam et al., 2008).
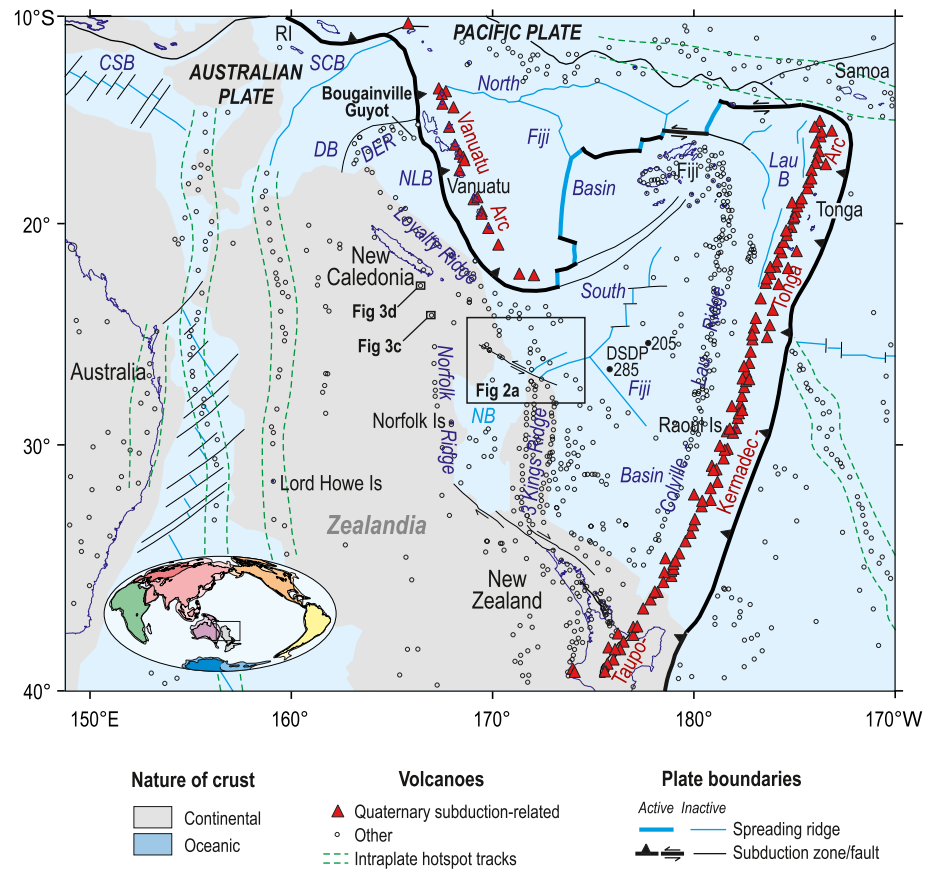
Figure 1. Regional volcanic-tectonic setting of the southwest Pacific Ocean. Oval inset shows area of main figure on a global continent map. The main VESPA study area, on the Loyalty and Three Kings Ridges is shown by the large rectangle: other dated samples shown by small rectangles and Bougainville Guyot. CSB, Coral Sea Basin; SCB, Santa Cruz Basin; RI, Rennell Island; DB, D'Entrecasteaux Basin; DER, D'Entrecasteaux Ridge, NLB, North Loyalty Basin; NB, Norfolk Basin. Map after Mortimer and Scott (2020); South Fiji Basin spreading ridge geometry from Herzer et al. (2011) and MacLeod et al. (2017).

3. VESPA Expedition

The VESPA (Volcanic Evolution of South Pacific Arcs) voyage of N/O *l'Atalante* was designed to fill key data gaps in knowledge of the geology of the submarine Loyalty and Three Kings Ridges in order to help test models of the tectonic development of the southwest Pacific (Mortimer & Patriat, 2016). The main 80,000 km^2 work area (Figures 1 and 2a) lies ~1,100 km north of Auckland, New Zealand, and ~800 km southeast of Nouméa. Previous work in this area (Figure 2a) comprised pioneering 1970s–80s surveys (e.g., Davey, 1982; Lapouille, 1977; Launay et al., 1982; Malahoff et al., 1982; Recy & Dupont, 1982; Watts et al., 1977) and more recent reflection seismic and multibeam bathymetry surveys (Bernardel et al., 2002; Herzer et al., 2011; Mauffret et al., 2001; Ramsay et al., 1997). Prior to the VESPA voyage, there were only two dated lavas in this area FAUST2-DR3 and TAN9912-DR9 (Figure 3a; Bernardel et al., 2002; Mortimer et al., 2007).

VESPA was a program of closely spaced dredge sampling, supported by seismic reflection profiling (Mortimer & Patriat, 2016). The work plan took advantage of the fact that the Loyalty and Three Kings Ridges are cut by the Cook Fracture Zone (CFZ), a sinistral strike slip fault of ~250 km lateral displacement (Herzer et al., 2011; Lapouille, 1977; Recy & Dupont, 1982). Importantly, the 1,000–1,500 m relief of the bathymetric walls of the CFZ allowed the expedition to acquire samples at different stratigraphic depths within the Loyalty and Three Kings Ridges. A total of 43 dredges were made on the voyage, nine on the Norfolk Ridge and 34 in the Loyalty Ridge-Three-Kings Ridge-Cook Fracture Zone area (Mortimer & Patriat, 2016; Mortimer et al., 2021; this paper; Figures 2 and 3).
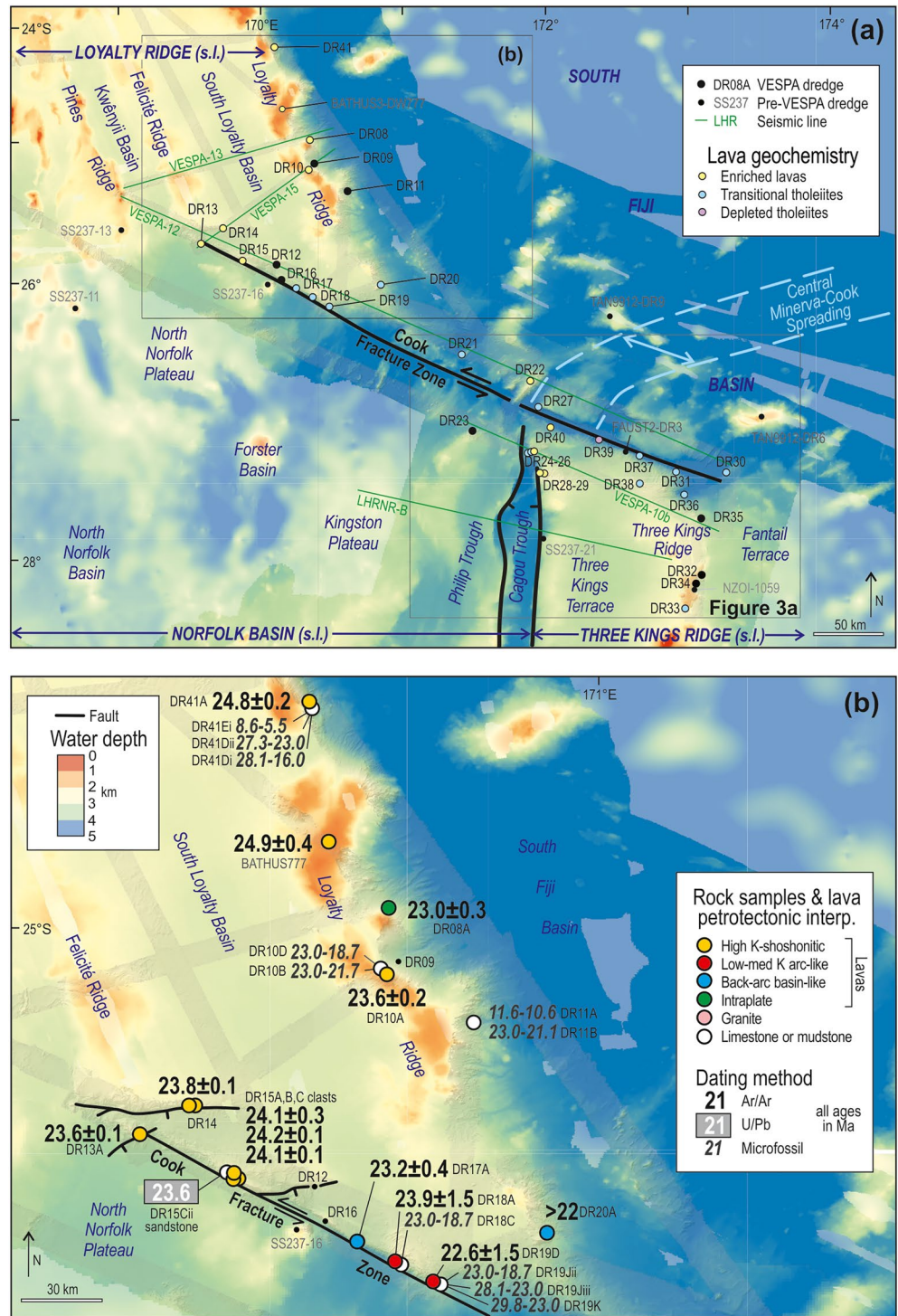
Figure 2. (a) Bathymetric and sample sites of the main VESPA expedition work area. Symbols indicate geochemical classification of lavas by Agranier et al. (2023). Labels show how the regional terms Loyalty and Three Kings Ridges, and Norfolk Basin (bold italic uppercase text) include smaller basins, troughs, terraces, and ridges (italic lowercase text). (b) More detailed bathymetric map showing sample sites in the Loyalty Ridge work area. Symbols indicate rock type and interpreted petrotectonic setting of lavas as explained later in this paper. Background bathymetry is from GEBCO Compilation Group (2019) supplemented by VESPA multibeam bathymetry tracks (shaded; Mortimer & Patriat, 2016). Tectonic information is from Herzer et al. (2011).
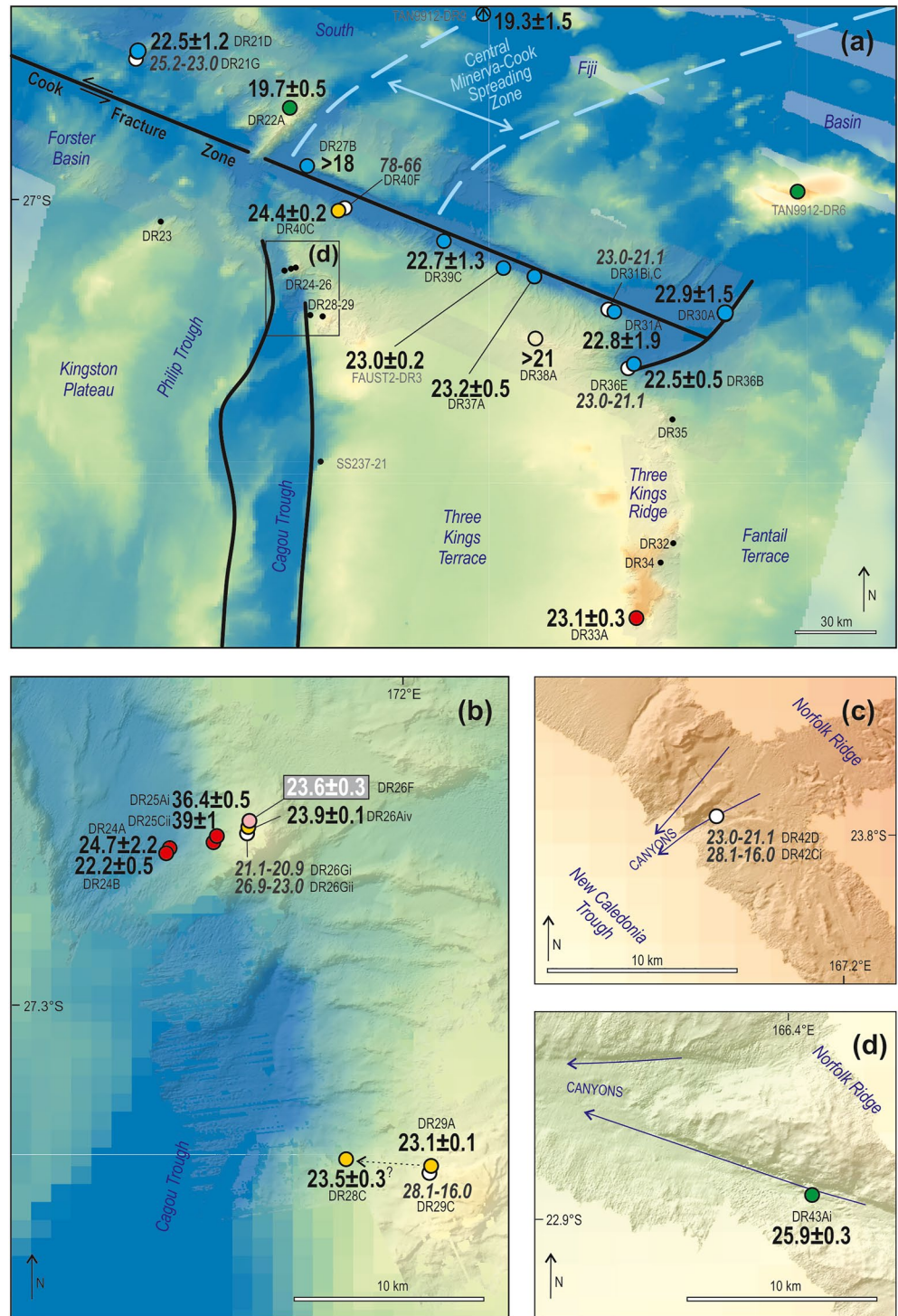
Figure 3. (a) Three Kings Ridge work area (box in Figure 2a). (b) Northern part of Cagou Trough. (c) VESPA site DR42 (Norfolk Ridge, see Figure 1). (d) VESPA site DR43 (Norfolk Ridge, see Figure 1). Colors and symbols as in Figure 2b.

Details of ship personnel, equipment, dredging procedures, multibeam bathymetric maps of dredge sites, sample photographs, shipboard descriptions of rocks, and portable X-ray fluorescence analyses are given in the cruise report (Mortimer & Patriat, 2016). Multibeam bathymetric mapping with a Kongsberg EM122 echosounder was used to position dredge tracks on appropriately oriented, steep rocky slopes and/or canyons. Typically, a rock dredge was dragged for ~500–1,000 m along the seabed before it was brought on deck. Quantities of rock recovered

ranged from 1 to 600 kg and were typically 30–100 kg. Onboard, samples were cut on a rock saw, examined with hand lens and binocular microscope, and sorted into different rock type categories. Each rock type in every dredge was given a unique field number. A total of c. 770 kg of rock was retained, and 235 individual samples cataloged. Splits of samples were sent to participating institutions for further work. The samples are archived in GNS Science's petrology and paleontology collections (Clowes et al., 2021; Strong et al., 2016) and are available for further study on request to GNS Science. In addition to the VESPA rocks, we dated two other samples for this paper (Figures 1 and 2). These are an andesite dredged from the Loyalty Ridge by the 1993 BATHUS3 cruise of N/O *l'Alis* (Figure 2b, Richer de Forges & Chevillon, 1996) and a rhyolite dredged from Bougainville Guyot (east end of the D'Entrecasteaux Ridge) on the 1985 SEAPSO cruise (Figure 1; Collot et al., 1992).

4. Analytical Methods

Dating by Ar/Ar methods at the University of California Santa Barbara, U.S.A (UCSB) followed procedures described in Gans (1997) and Mortimer et al. (2014). One sample was dated by Ar/Ar methods at the U.S. Geological Survey, Menlo Park (cf. Calvert & Lanphere, 2006). All Ar/Ar ages in this paper are reported relative to a Fish Canyon sanidine age of 28.198 Ma. U/Pb dating of zircon was done by LA-ICP-MS (Laser Ablation-Inductively Coupled Plasma-Mass Spectrometry) methods at the University of Otago, Dunedin, New Zealand following methods described in Mortimer et al. (2015). A Resonetics RESOlution M-50-LR excimer laser ablation system was used with a spot diameter of 33 μm, 5 Hz repetition rate and 40 s acquisition time. Isotopes were measured on an Agilent 7500cs quadrupole ICP-MS. Fractionation of Pb, Th and U was corrected using the TEMORA-2 zircon standard. TEMORA-2, R33, and NIST glass 610 were measured during analytical sessions and used to calculate correction factors. Foraminifera and radiolarian extraction and examination at GNS Science Lower Hutt, New Zealand followed standard methods (Crundwell et al., 2016). Electron microprobe elemental maps and analyses of the groundmasses of selected dated volcanic rocks were conducted at UCSB. A detailed description of the procedures and approaches used to obtain optimal Ar/Ar results is outlined in Section 5 below. Further details of other analytical methods and equipment used are given in Supporting Information S1. Throughout the paper, all radiometric age errors are quoted as ±2σ and/or 95% confidence level and the timescale of Raine et al. (2015) is used.

5. $^{40}Ar/^{39}Ar$ Geochronology of Submarine Basalts

5.1. General Considerations

Dredged mafic submarine lavas present special problems for Ar/Ar dating. These include absence of stratigraphic control and context, and limited choice of datable material (i.e., rock type, phenocryst content, grain size and freshness). Other problems include the very low K/Ca ratios of plagioclase phenocrysts, low overall K content of the whole rock and common replacement of K-rich groundmass crystalline phases and interstitial glass by secondary minerals such as clays, zeolites, oxides. In rocks that lack a suitable phenocryst phase, the only option is to attempt to date the microcrystalline groundmass. Such fine-grained and composite aggregates of primary and secondary phases commonly yield complex $^{40}Ar/^{39}Ar$ age spectra that are difficult to interpret because of varying degrees of hydrothermal alteration, low temperature argon loss, low radiogenic yields, low K contents, and reactor-induced recoil of ^{39}Ar, ^{37}Ca, and ^{36}Ar. In subaerial basalts these problems are minimized by sampling the most slowly cooled holocrystalline interior of thick lava flows that show the least amount of alteration (e.g., Gans, 1997). With dredged rocks, dating must be attempted on a very limited selection of less-than-ideal samples such as the quenched and vesicular upper portions of lavas, and/or samples that often show substantial clay alteration.

The principles of interpreting $^{40}Ar/^{39}Ar$ step heating results to obtain rock ages have been investigated for more than 50 years (e.g., Dalrymple & Lanphere, 1974; Turner, 1971), and dating principles are explained in textbooks such as McDougall and Harrison (1999) and Dickin (2005). A review paper by Schaen et al. (2021) addressed technical matters of irradiation, standards, monitors, and statistical treatment of data, but paid less attention to sample selection strategies, screening and sample preparation, and interpretation of "disturbed" age spectra. Many studies have noted that incremental heating $^{40}Ar/^{39}Ar$ analyses from whole rock or groundmass separates of fine-grained mafic rocks often do not yield straightforward plateaus (e.g., Fleck et al., 2014; Gans, 1997; Iwata & Kaneoka, 2000). While plausible explanations and recommendations for interpreting these "disturbed" spectra have been offered, rarely is a rigorous assessment made as to how potassium is actually distributed between various primary and secondary groundmass phases and how this might influence the resultant age interpretation.

Natural samples rarely behave according to theory and are often difficult to interpret, especially when dealing with many of the complexities outlined above. In this paper, we address problems with dating the very fine-grained to glassy groundmass of relatively low K and variably altered basalts and basaltic andesites.

5.2. Analytical Approach

Hand specimens of all VESPA lavas were examined on board ship to identify those possibly suitable for argon geochronology. Post-cruise petrographic inspection eliminated samples that were too altered to consider dating, for example, where matrix was mostly replaced by secondary minerals and where plagioclase was substantially altered. Petrographic examination at high optical magnifications (20X and 40X objectives; Supporting Information S2) allowed visual estimates of what groundmass phases (e.g., plagioclase, pyroxene, glass, oxides, secondary clays, etc.) were present and their approximate proportions.

Rocks that passed these initial screenings underwent phenocryst and groundmass separation. Pure separates of plagioclase and other phenocryst phases were obtained from sieved fractions (125–250 μm) using standard density and magnetic mineral separation techniques described in Mortimer et al. (2014); plagioclase phenocrysts were handpicked and had no adhering groundmass material. Groundmass concentrates from 125 to 250 μm sieve fractions were obtained by light magnetic separations which selectively removed phenocrysts and secondary phases. The groundmass concentrates then underwent intensive ultrasonic cleaning for several hours in repeated changes of deionized water to remove secondary clay and zeolite. No samples were treated with acid, as we have found from past experience that this tends to greatly reduce radiogenic yields by increasing atmospheric contamination due to increased surface area; clays, zeolite and carbonate can be satisfactorily removed by magnetic separation and ultrasonic cleaning alone. Importantly, whenever possible, both plagioclase phenocrysts and groundmass from the same sample were separated for dating to provide a mutual crosscheck of the Ar/Ar results. Our previous experience (e.g., Mortimer et al., 1998, 2007, 2014, 2018, 2021) has demonstrated that it is not always possible to predict in advance whether groundmass or phenocrysts would yield the best result.

The $^{40}Ar/^{39}Ar$ ages were obtained by incremental heating experiments on both phenocryst and groundmass separates. There was a wide range in complexity of step heating spectra, reflecting the multiple issues mentioned in Section 5.1 above. Some plagioclase phenocrysts had very low K/Ca <0.005 and low signal/noise ratios; these required a large correction for the interfering isotopes of Ca-derived ^{36}Ar and ^{39}Ar. Normally, such material would be regarded as unsuitable for Ar/Ar dating. However, by taking great care to monitor uncertainties in system blanks, reactor constants (especially for Ca), mass discrimination and tailing corrections, meaningful (albeit imprecise) ages were obtained from these low-K plagioclases. Many incremental heating experiments use a 500–1300°C temperature range. Our experience in dating groundmass concentrates from mafic lavas has consistently shown that the loosely held argon released at the lowest temperatures (350–550°C) and the highly retentive argon released at the highest temperatures (≥1150°C) is both analytically problematic and are almost never used in age interpretations (e.g., Nauert & Gans, 1994).

Specifically, the low T gas yields apparent ages that can either be too old (due to recoil) or too young (due to Ar loss from non-retentive phases) and include hydrocarbons that contaminate the mass spectrometer. Gas released at the highest T steps commonly also yields ages that can be either too young (due to recoil) or too old (excess Ar trapped in the most retentive phases). In the latter case, steps are associated with elevated ^{37}Ar signals and a substantial drop in apparent K/Ca ratios due to the degassing of highly retentive calcic phases (pyroxenes and the cores of plagioclase crystals). All the step heating experiments on groundmass reported here commenced with a 30-min degassing of each sample at ∼500°C, followed by 9–10 incremental heating steps spanning 600–1100°C, and a final high temperature degassing of any residual gas. Thus, our approach was to focus on the middle T fraction of the gas that is the largest volume and analytically most meaningful.

As our VESPA Ar/Ar dating work proceeded, it was clear that different groundmass separates were yielding very different results in terms of the quality of the data as revealed by the shape and complexity of the resultant age spectra. We set out to better understand this variability by defining the different K reservoirs in primary and secondary groundmass phases. To do this, we conducted a detailed electron microprobe investigation of eight samples representing a range of petrographic textures and argon spectrum types (Table 1, Figure 4, Supporting Information S3 and S4). Quantitative X-ray 10 element (K, Na, Ca, Fe, Mg, Ti, Al, Si, Cr, Mn) maps of representative 600 × 600 μm groundmass areas supplemented by quantitative point analyses of the principal K-bearing domains for each of these sample provided detailed information on the proportions of groundmass phases present, and their precise chemical composition.

Table 1
Summary of New Ar/Ar Ages From 33 VESPA Samples

VESPA #	GNS P#	Long (°E)	Lat (°S)	Depth (m)	Rock description	Material dated	Preferred age (Ma)	±2σ	Spectrum	Plateau	Other dated material	Trace element compn.	Petro-tectonic interp.
Quality rank A: simple plateaus, high precision ages													
DR10A	84607	170.3192	25.1513	1,500	Basaltic andesite	plag	23.60	0.24	1	Y	gm	Enriched	Shosh
DR13Aii*	84621	169.5488	25.6681	2,700	Basaltic trachyandesite	gm	23.62	0.10	1	Y	plag	Enriched	Shosh
DR14Ai*	84629	169.6967	25.5786	2,100	Trachyandesite	gm	23.81	0.10	1	Y	plag	Enriched	Shosh
DR15A	84639	169.8381	25.8163	2,200	Basaltic and. bldr from pebbly sst	plag	24.14	0.26	1	Y	gm	Enriched	Shosh
DR15B	84640	169.8381	25.8163	2,200	Trachyte bldr from pebbly sst	bi	24.20	0.10	1	Y	plag	Enriched	Shosh
DR15Ci	84641	169.8381	25.8163	2,200	Basaltic and. cobble fr pebbly sst	plag	24.12	0.12	1	Y	gm	Enriched	Shosh
DR26Aiv	84722	171.9461	27.2030	2,400	Andesite	bi	23.89	0.10	1	Y	hbl, plag	Enriched	Shosh
DR29A	84744	172.0336	27.3615	2,100	Basaltic trachyandesite	gm	23.10	0.10	1	Y	-	Enriched	Shosh
Quality rank B: high age confidence, fairly low uncertainties													
BATHUS-777	na	170.0998	24.7186	800	Basaltic andesite	bi	24.9	0.4	1	Y	-	Enriched	Shosh
DR17Aii*	84658	170.2254	26.0258	3,500	Doleritic basalt joint block	plag	23.2	0.4	1	Y	-	Trans.	BABB
DR24Bii	84707	171.9098	27.2128	3,700	Doleritic basalt	plag	22.2	0.5	1	Y	gm	Trans.	Arc
DR28C	84740	171.9934	27.3573	3,000	Basalt	gm	23.5	0.3	3	N	-	Enriched	Shosh
DR33Ai	84761	173.0522	28.3423	1,400	Basalt	gm	23.1	0.3	2	Y	plag	Trans.	Arc
DR37Ai	84775	172.7205	27.2333	4,200	Columnar-jointed aphyric basalt	gm	23.2	0.5	1	Y	-	Trans.	BABB
DR40C*	84792	172.0745	27.0257	3,700	Basaltic and. volc breccia clast	plag	24.4	0.2	2	Y	gm	Enriched	Shosh
DR41Aii	84798	170.0669	24.2663	2,900	Basaltic joint block with glassy rind	gm	24.8	0.2	3	N	-	Enriched	Shosh
DR43Ai	84812	166.4114	22.8864	2,299	Basaltic trachyandesite	plag	25.9	0.3	1	Y	-	Trans.	Intraplate
SEAPSO-D2C	na	166.7198	16.1319	3,400	Rhyolite	gm	40.6	0.4	3	N	plag	Trans.	Arc
Quality rank C: disturbed spectra and/or very low K/Ca, but interpretable													
DR08A	84602	170.3263	24.9381	2,300	Aphyric basalt/ basanite	gm	23.0	0.3	2	N	-	Enriched	Intraplate
DR18Avii*	84670	170.3474	26.0882	3,400	Basalt joint block in basaltic brecc	plag	23.9	1.5	1	Y	gm	Trans.	Arc
DR19D	84678	170.4683	26.1529	3,000	Basalt	plag	22.6	1.5	1	Y	gm	Trans.	Arc
DR21D	84691	171.4284	26.5021	3,400	Aphyric basalt	gm	22.5	1.2	5	N	-	Trans.	BABB
DR22A	84694	171.9271	26.6865	2,800	Pillow basalt with glassy rind	gm	19.7	0.5	3	Y	-	Enriched	Intraplate
DR24Ai	84705	171.9098	27.2128	3,700	Basaltic and. ?pillow w glass rind	plag	24.7	2.2	1	Y	-	Trans.	Arc
DR25Ai	84711	171.9309	27.2067	3,000	Aphyric basaltic trachyandesite	gm	36.4	0.5	2	N	-	Trans.	Arc

Table 1
Continued

VESPA #	GNS P#	Long (°E)	Lat (°S)	Depth (m)	Rock description	Material dated	Preferred age (Ma)	±2σ	Spectrum	Plateau	Other dated material	Trace element compn.	Petro-tectonic interp.
DR30Ai	84749	173.3406	27.3485	4,000	Basalt with glassy rind	plag	22.9	1.5	1	Y	gm	Trans.	BABB
DR31Ai	84754	172.9846	27.3491	3,900	Basalt with glassy rind	plag	22.8	1.9	1	Y	gm	Trans.	BABB
DR36B	84771	173.0451	27.5167	3,900	Columnar-jointed aphyric basalt	gm	22.5	0.5	4	N	-	Trans.	BABB
DR39C*	84785	172.4261	27.1165	4,000	Doleritic basalt	plag	22.7	1.3	2	Y	-	Depleted	BABB
Quality rank D: highly disturbed spectra, low K/Ca and/or low %rad													
DR20A	84688	170.8399	25.9939	2,700	Weathered basalt	gm	>22	2	5	N	-	Trans.	BABB
DR25Cii*	84714	171.9309	27.2067	3,000	Doleritic basaltic andesite	plag	39	1	5	N	-	Trans.	Arc
DR27B	84733	171.9853	26.8770	3,800	Basalt with palagonite rind	gm	>18	2	5	N	-	Trans.	BABB
DR38A	84781	172.7225	27.4344	2,100	V altered hyaloclastite breccia	gm	>21	1	5	N	-	Trans.	?

Note. See Figures 2 and 3 for maps, Supporting Information S5 for mineralogy and individual age results of all 49 Ar/Ar dated separates, and Supporting Information S6 for raw Ar/Ar data tables, spectra and isochron plots. Plag, plagioclase; hbl, hornblende; bi, biotite; gm, groundmass. Longitude, latitude and depth are estimates of mid-point of dredge track on sea floor, coordinates are in WGS84 decimal degrees.

5.3. Groundmass Petrography

The groundmasses of dated samples range from mostly glassy to holocrystalline and display varying degrees of alteration (Supporting Information S5). Primary groundmass crystalline phases nearly always include plagioclase, clinopyroxene, and iron titanium oxides, and may also include minor amounts of olivine, orthopyroxene, and late crystallized sanidine. Interstitial glass may be entirely fresh, but more commonly is partially or completely altered to fibrous aggregates of Fe- and K-rich clays, Fe-oxides, and zeolites (Figure 4). These primary and secondary phases occur in highly variable proportions for different samples, ranging from holocrystalline coarse-grained (75–200 μm) interlocking fresh crystal aggregates of plagioclase-pyroxene-olivine in a diabasic texture, to highly vesicular and glassy groundmass samples containing less than 25% microlites of flow-aligned acicular plagioclase (25–75 μm long and 4–10 μm wide) and tiny blebs of pyroxene and oxide in a matrix of glass or its alteration products. Phenocryst phases include plagioclase ± clinopyroxene ± olivine and account for anywhere from a few percent to 30% of total rock volume.

5.4. Groundmass K Reservoirs From Element Mapping

Any interpretation of $^{40}Ar/^{39}Ar$ ages implicitly assumes a knowledge of exactly what phase or phases are being dated. This is self-evident for pure phenocryst separates, but far less so for the various fine-grained polycrystalline aggregates that make up the groundmass of mafic lavas. We used detailed electron microprobe studies to assess exactly which phases contribute to the $^{40}Ar/^{39}Ar$ ages we obtain from groundmass samples.

Our element maps and microprobe analyses of eight representative groundmass samples from VESPA lavas were used to calculate how K and Ca are distributed in different groundmass phases (Table 2, Supporting Information S4). The primary K reservoirs in all samples are plagioclase, interstitial glass and late crystallizing sanidine. Secondary K reservoirs include clay and zeolite. The distribution of K varies enormously between samples (Table 2). In well-crystallized groundmass samples, a large percentage (35%–85%) of the total K resides in groundmass plagioclase (and in sanidine in more potassic rocks), whereas in the quenched lavas, 80%–90% of the K resides either in interstitial glass or its clay and zeolite alteration products. Groundmass plagioclase in all samples is inevitably zoned from more calcic (An_{50-75}) cores to more sodic (An_{30-50}) rims, a zonation that is accompanied by a marked increase in wt% K and K/Ca ratios. Groundmass plagioclase cores may contain as little as 0.02 wt% K with K/Ca ratios as low as 0.001, to as much as 0.5 wt% K (with K/Ca ~0.06). Similarly,
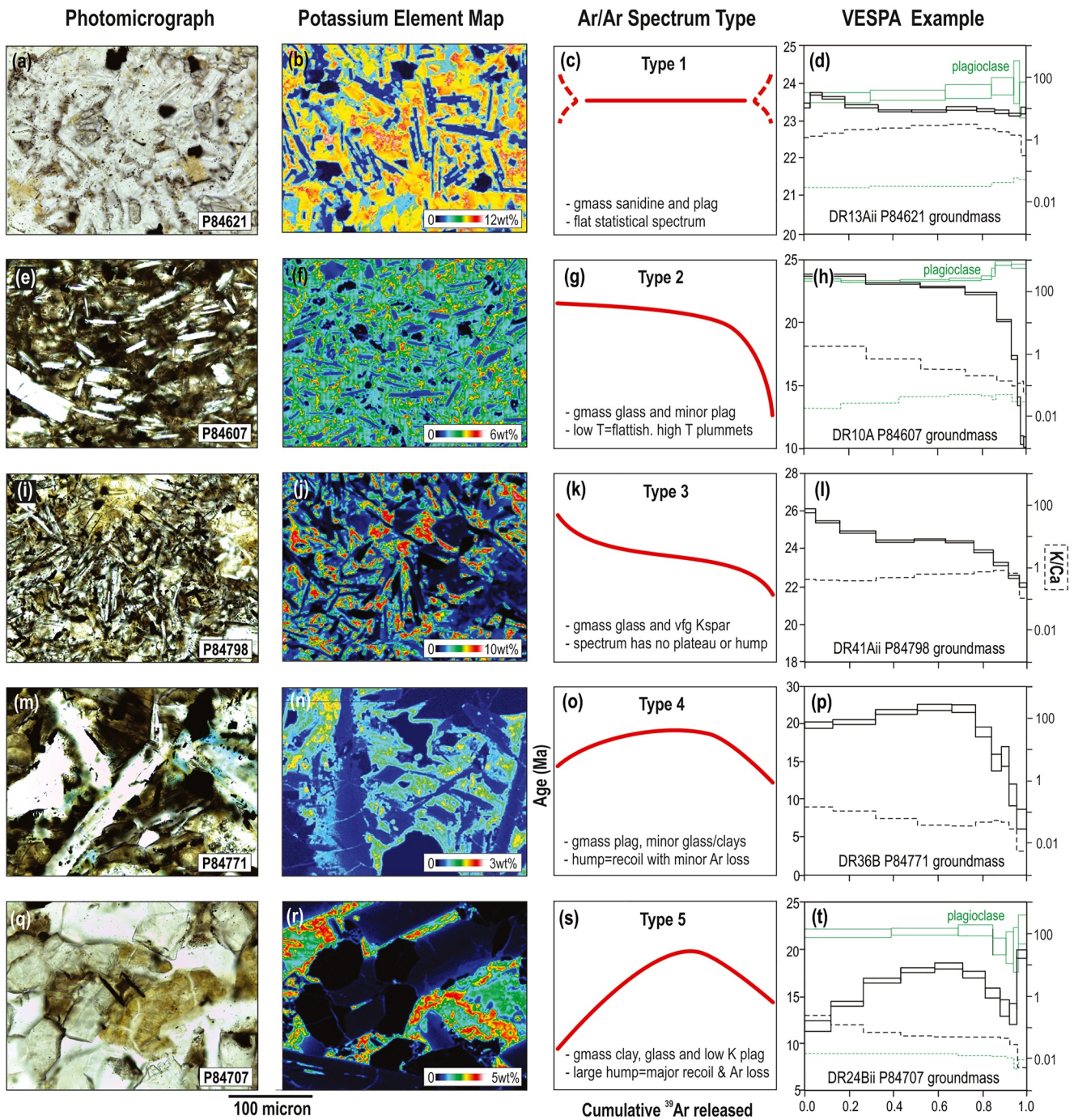
Figure 4. Groundmass textures, mineralogy, potassium distribution and bulk K/Ca for specific VESPA samples related to five broad types of $^{40}Ar/^{39}Ar$ degassing spectra. (a–d) Type 1 flat spectrum of DR13Aii. (e–h) Type 2 descending staircase spectrum of DR10A. (i–l) Type 3 S-shaped spectrum of DR36B. (m–p) Type 4 shallow hump spectrum of DR24Bii. (q–t) Type 5 steep hump spectrum of DR41Aii. Note that photomicrographs and X-ray element maps are at the same scale but of different sample parts. See Supporting Information S4 for additional element maps and complete spot analyses.

K contents of plagioclase rims range from c. 0.1 to 1.0 wt% K, with K/Ca ratios ranging from 0.005 to 0.15. Although the K-rich rims are often quite thin (1–5 μm), they typically account for the majority (50%–80%) of the total K residing in plagioclase. Interstitial glass and the high-K clays that replace them have significantly higher K contents (1.0–2.5 wt%) and K/Ca ratios of 0.5–2.0. Sanidine (and some high K zeolites) have even higher K contents (3–9 wt%) and K/Ca ratios of 3–10. It is important to keep in mind that significant fractions of the loosely held clays and zeolites noted in Table 2 were likely removed during ultrasonic cleaning of the groundmass

Table 2
Volume % of Potassic Phases in Eight VESPA Lavas

Dredge GNS P#	DR41Aii 84798	DR36B 84771	DR33Ai 84761	DR27B 84733	DR24Bii 84707	DR13Aii 84621	DR10A 84607	DR08A 84602	~K/Ca
Spectrum type	5	3	1	5	4	1	2	4	
Pyroxene (vol%)		3	2		3				0.001
Plagioclase core	8	10	33	5	11	5	3	37	0.04
Plagioclase rim	26	24	45	9	8		14	44	0.14
Glass	16		16		3	8	69		1.6
Sanidine	50					87			9
Clay		56		53	75			19	1.3
Other high K phase		7	4	33			14		2.5
Total	100	100	100	100	100	100	100	100	

Note. Values in representative 600×600 μm groundmass areas are normalized to 100% non-potassic phase and void-free. Based on electron microprobe element mapping (Supporting Information S3).

separates, thus removing a portion of the original K. Therefore, the quantitative K-budgets in the separates that were subsequently irradiated and dated may be different from what was present in the analyzed sample.

5.5. Types of Groundmass Ar/Ar Spectra and Their Interpretation

A cursory inspection of all age spectra from groundmass separates of the dredge samples collected in this study (Supporting Information S6), as well as from our previous studies of southwest Pacific submarine lavas (e.g., Mortimer et al., 1998, 2007, 2015, 2021) reveals that they tend to fall into five distinct spectral types (Figure 4). In the best-cases, incremental heating experiments of groundmass yields reasonably flat age spectra (Type 1 in Figure 4), where most (>70%) of the gas released defines a plateau of successive steps whose age errors are within two sigma of each other, resembling what is commonly obtained from separates of fresh K-bearing phenocryst phases. In Type 2 spectra, apparent ages start relatively high, steadily decrease over the first 50%–80% of the gas released, and then plummet downward to much younger ages at the highest temperature steps. Type 3 spectra have ages that initially step down over the first 10%–30% of the gas released, flatten into a well-defined plateau in the central part of the spectrum, and then step down again at the highest temperatures. Type 4 and Type 5 are both hump-shaped spectra (Figure 4), with ages that initially climb, reach a maximum in the central part of the age spectrum, and then step down at the highest temperatures, the main difference being that Type 4 are somewhat broader humps with a well-defined flat "mini-plateau" at the top of the hump. Each of these different spectrum types commonly has a characteristic associated K/Ca distribution (Figure 4), and the deviations from a simple flat age spectrum for Types 2–5 can be explained in terms of varying contributions from reactor induced recoil, partial argon loss in the natural environment, and a trapped "excess argon" component. Inverse isochron plots help with age interpretation as "excess Ar" steps lie well off isochron lines.

Recoil is the redistribution of ^{39}Ar and ^{37}Ar because of the neutron flux during irradiation and is important only on very small length scales (≤ 1–2 μm) (e.g., Fleck et al., 2014; McDougall & Harrison, 1999). During irradiation some fraction of the ^{39}Ar atoms may be dislodged from high K sites (e.g., K-rich rims of plagioclase or K-rich clays and zeolites), losing some to the atmosphere and embedding others in lower K sites (e.g., in the interiors of plagioclase crystals or in adjacent refractory non-K bearing phases). A similar recoil redistribution is expected for Ca-derived ^{37}Ar. The predictable consequence of recoil is that the earliest released argon (from the smallest grains and outer rims of larger grains) will have elevated $^{40}Ar/^{39}Ar$ ratios and thus older apparent ages, whereas the argon released at highest temperatures will yield anomalously younger ages due to the presence of excess ^{39}Ar. Similarly, in very calcic phases, recoil of ^{37}Ar may yield slightly lower $^{37}Ar/^{39}Ar$ (apparent K/Ca ratios), at low T balanced by slightly elevated K/Ca at high T in the spectrum. On inverse isochron plots, ^{39}Ar recoil often yields loops instead of lines.

Argon loss may be the consequence of diffusive loss of the ^{40}Ar daughter product from non-retentive phases (e.g., glass) or the replacement of primary igneous phases by the new growth of distinctly younger secondary K-bearing phases—in both cases yielding younger apparent ages (e.g., McDougall & Harrison, 1999). These younger ages

will be most evident in the gas released early in the incremental heating experiment that is coming from the outer portions of primary phases and the generally non-retentive secondary phases. Excess argon is the ambient argon that is trapped during initial crystal growth having an initial $^{40}Ar/^{36}Ar$ ratio that is distinctly higher than normal atmospheric argon. This yields anomalously old ages and is most evident in gas released at the highest temperatures from highly retentive and very low K/Ca sites such as the cores of plagioclase phenocrysts or pyroxenes.

None of the above complexities are mutually exclusive. For example, K-rich rims on plagioclase, tiny patches of interstitial sanidine and glass, and secondary K-rich clays and zeolites would be susceptible to both argon loss and reactor induced recoil, such that the low temperature steps might be either anomalously old (recoil dominant) or young (argon loss dominant). Similarly, ages at the highest temperature steps might either increase (excess argon) or decrease (recoil), depending on which is dominant. Notably, much of the very loosely held argon situated in K-rich clays, zeolites, and/or micron-scale blebs and rims of sanidine and glass was not analyzed in our incremental heating experiments as it was pumped away during the initial degassing. This low temperature argon is of little use, being the most severely affected by recoil and argon loss, and often contaminated by excessive adsorbed atmospheric argon (low radiogenic yield) and hydrocarbons whose masses overlap the target argon isotopes. Indeed, one of the principal advantages to obtaining $^{40}Ar/^{39}Ar$ ages from groundmass separates using well-calibrated incremental heating is that it allows us to selectively degas and analyze different argon domains within each sample and focus our analytical efforts on those primary K reservoirs and phases that are least affected by some of the interferences outlined above.

5.5.1. Type 1 Spectrum—Flat With a Simple Plateau

Type 1 groundmass samples like DR13Aii (P84621) (Figure 4a) generally have elevated K/Ca ratios and high analytical precision such that there is little ambiguity in their age assignment. This sample contains a very fresh, mostly crystalline groundmass composed of interlocking 25–75 μm crystals of plagioclase (30% $An_{47–52}$), clinopyroxene (7%), and Fe-Ti oxide (4%) with abundant interstitial sanidine (45%) in patches up to 40 μm across. Minor phases include pale brown glass (10%) and traces of biotite and calcite (<2%). Of the total potassium present, c. 87% is held in sanidine (Table 2) with K/Ca ~10, the remainder is in groundmass plagioclase and glass. The groundmass argon spectrum (Figure 4d) yields slightly older ages in the lowest temperature steps due to the recoil loss of ^{39}Ar from small non-retentive glass domains, a broad central plateau associated with high K/Ca ratios during the release of argon from both interstitial sanidine and plagioclase, and a slight drop in ages associated with lower K/Ca ratios at the highest temperatures due to recoil addition of ^{39}Ar to the more retentive plagioclase cores and pyroxene. The straightforward weighted mean plateau age (WMPA) (McDougall & Harrison, 1999) calculated from most of the argon reflects the crystallization age of the groundmass—in particular, the age of the fresh interstitial sanidine that holds most of the K. Note that the groundmass in this sample yields a more precise estimate of the age (23.62 ± 0.10 Ma) than the phenocrystic plagioclase (24.07 ± 0.18 Ma—Supporting Information S5 and S6) because of the inherently better precision associated with the higher K content and much lower Ca correction.

5.5.2. Type 2 Spectrum—Progressively Decreasing Ages

Type 2 spectra such as that of DR10A (P84607) groundmass tend to show radiogenic argon release at lower temperatures than most other groundmass samples and display a "descending staircase" type spectrum that starts relatively flat and descends steeply at higher temperatures (Figure 4h). DR10A is a porphyritic basalt containing ~25% phenocrysts of plagioclase, clinopyroxene, and completely iddingsitized olivine. The groundmass consists of 28% fresh flow-aligned plagioclase crystals and a few % each of pyroxene, olivine, and Fe-Ti oxide crystals in a fresh glassy matrix (Figure 4e). In addition, there is ~4% of an unidentified late-stage high K phase that is either sanidine or K-rich secondary clay/zeolite that occurs as tiny interstitial blebs only a few microns in diameter. The plagioclase laths are only 5–20 μm wide and are zoned from calcic cores to sodic rims. More than two-thirds of the total K is held in the groundmass glass, with the remainder mostly split between the late K-rich alteration phase and the thin sodic rims on plagioclase (Table 2, Figure 4f).

Apparent ages of the low temperature gas steps are about 24 Ma. They initially decrease gradually but drop abruptly at higher temperatures to as young as 10 Ma. The age decrease is matched by decreasing K/Ca ratios from 1.6 to 0.06. The relatively flat low to middle *T* part of the spectrum yields a weighted mean age of 23.2 ± 0.5 Ma that is within error of the much better defined WMPA of 23.60 ± 0.24 Ma obtained from phenocrystic plagioclase. The early analytical steps (600–750°C, K/Ca = 0.2–1.5) mainly represent degassing of fresh groundmass glass and

plagioclase rims. Higher temperature steps record an increasing contribution from plagioclase (K/Ca = 0.06–0.2) with apparent ages lowered by excess ^{39}Ar, possibly due to recoil from adjacent high K glass sites.

5.5.3. Type 3 Spectrum—S-Shape With Central Flat Part

The porphyritic basaltic andesite sample DR41Aii (P84798) provides a typical example of an S-shaped ground-mass spectrum (Figure 4l). The groundmass contains 50% acicular plagioclase (25–50 μm long and 2–10 μm wide), 20% prismatic ortho- and clinopyroxene, 18% pale brown interstitial glass with minor clay alteration, 9% tiny blebs of late-stage interstitial sanidine and 2% Fe-Ti oxides (Figure 4i). The sample is quite K-rich; 50% of the potassium is in sanidine which has ~8.8 wt% K with K/Ca = 3–8; 26% is in the sodic rims (An_{45-50}) of plagioclase which has c. 1.8 wt% K with a K/Ca = 0.6–0.8, 7.5% is in the calcic cores (An_{65-75}) of plagioclase which has c. 0.45 wt% K with K/Ca ~0.05, and 16% is held in glass partly altered to clay which has c. 1.5 wt% K with K/Ca ~0.7.

The age spectrum is a classic recoil pattern, with ages that step down over the initial 30% of the gas released, flatten through the middle 50%, and descend again at high T. The apparent K/Ca ratios are relatively constant, but climb from 0.35 to 0.65, and then drop abruptly at the high T. Much of the argon related to the 1–2 μm sanidine blebs was likely pumped away during initial degassing (the K/Ca is never high enough to be explained solely by sanidine) and most of the spectrum reflects simultaneous degassing of glass and plagioclase. Older but decreasing ages early in the incremental heating are a consequence of recoil induced ^{39}Ar loss from outer rims of plagioclase. The central flat portion of the spectrum yields a weighted mean age of 24.78 ± 0.10 (not a statistical plateau) representing 44% of the total gas released from plagioclase rims and cores with perhaps a minor contribution from glass. Decreasing ages in the highest T steps reflect degassing of more retentive plagioclase cores, whose ages have been reduced by the addition of excess ^{39}Ar. The modest climbing of apparent K/Ca over the middle part of the spectrum likely represents recoil induced redistribution of ^{37}Ar—especially in plagioclase. Though this sample is very fine-grained with a significant glass component, a reasonably good age was obtained because of the high overall K content, and the fact that K was distributed between the viable reservoirs of relatively high-K plagioclase and fresh glass.

5.5.4. Type 4 Spectrum—Shallow Hump-Shape With a Reasonably Flat Top

Sample DR36B (P84771) is a quenched basalt with abundant vesicles and a hypocrystalline groundmass containing 68% interlocking swallow-tailed/skeletal plagioclase laths (150–300 μm long and 30 μm wide), 15% pyroxene (50–100 μm), 4.5% Fe-Ti oxides, and 12% brown interstitial glass partially altered to clay (Figure 4m). The potassium is distributed as follows: c. 10% is in the An_{58-67} plagioclase cores which have ~0.06 wt% K and K/Ca = 0.008; 24% is in An_{25-40} plagioclase rims with ~0.25 wt% K and K/Ca = 0.09; 56% is in interstitial glass and Fe-rich clays with an average 1.4 wt% K and K/Ca = 1.25; and ~7% is in an unknown high-K phase with ~1.8 wt% K, and K/Ca = 1.0.

It is likely that much of the argon associated with the relatively high K, but non-retentive, glass and clay were removed during ultrasonic cleaning and initial sample degassing. The analyzed groundmass separate yields a broad hump-shaped spectrum, with a flat "mini-plateau" at the top of the hump, followed by rapidly decreasing ages at the highest temperatures (Figure 4p). Apparent K/Ca ratios steadily drop from 0.15 at the lowest T step to a central portion where they level at ~0.045, before dropping to 0.005 at the highest T. The early climbing part of the spectrum records degassing of glass/clays and plagioclase rims, with an increasing contribution from the latter. The young apparent ages from these reservoirs probably reflect both argon loss and recoil, but the former dominates. The best estimate of the sample age (22.5 ± 0.5 Ma) comes from the flat top of the hump reflecting gas derived primarily from both plagioclase rims and cores. The drop in ages at highest temperatures could reflect recoil induced excess ^{39}Ar added to low K plagioclase cores. Despite extensive recoil and argon loss, a meaningful age was obtained from this sample because a sufficient percentage of the K resides in the groundmass plagioclase, and the incremental experiment was able to effectively isolate and analyze the gas coming from the high K rims of this plagioclase.

5.5.5. Type 5 Spectrum—Steep Hump-Shape With No Obvious Flat Part

The groundmass of sample DR24Bii (P84707) is coarser-grained (50–250 μm) compared to most other VESPA samples, and consists of 45% interlocking plagioclase laths, 33% granular clinopyroxene, 2.5% Fe-Ti oxides, and 16% Fe-rich clays replacing intersertal glass and olivine (Figure 4q). The potassium is held in four distinct reservoirs (Table 2). Secondary clays account for 75%, averaging 2.5–4.0 wt% K and K/Ca = 2–6. Calcic cores

of plagioclase account for 11% but have very low K concentrations (~0.15 wt%) and K/Ca ≤0.02. Sodic rims on plagioclase account for an additional 8% with a somewhat higher K of 0.5 wt% and K/Ca ~0.15. The residual glass holds 3% with typically ~0.8 wt% K and K/Ca = 1.5.

The very strongly hump-shaped spectrum climbs from 10 Ma to a maximum of 18.6 Ma and then descends again at higher temperatures, with no two contiguous steps yielding concordant ages (Figure 4t). A low precision, but reasonably well-behaved separate of plagioclase phenocrysts from the same sample yielded a WMPA of 22.2 ± 0.5 Ma, which we take as the best estimate of the age for this sample. This is significantly older than even the oldest apparent age from the top of the hump from the groundmass. The shapes of the groundmass age and K/Ca spectra suggest that the early climbing part of the spectrum reflects simultaneous degassing of residual clay and glass (both of which experienced significant argon loss) with an ever-increasing contribution from the rims of groundmass plagioclase. The oldest ages were from the central part of the spectrum (43%–81% of the cumulative ^{39}Ar released, at 750–850°C) and is likely coming from both plagioclase cores and rims given the uniform K/Ca values of ~0.06. However, these ages are still too young to be primary because of the continued contribution from the K-rich non-retentive phases that experienced argon loss. At the highest temperatures, ages drop precipitously as do the K/Ca ratios, reflecting the degassing of refractory plagioclase cores and pyroxene, with their attendant excess ^{39}Ar induced by recoil. At first glance, this sample seems like it would be an excellent candidate for dating (coarse-grained, fresh primary igneous phases) but it is quite problematic because it has a very low overall K content, and much of the K that is present is held in non-retentive fine-grained clays that, despite ultra-sound treatment, seemingly were not removed during sample preparation.

5.5.6. Groundmass Age Spectra Interpretations: Key Points

The best groundmass spectra, Type 1, are obtained from fresh, mostly crystalline groundmass where most of the K is situated in groundmass feldspar. It helps if the rock is a reasonably high-K whole rock composition to begin with. The next best, Type 2, spectra are obtained from samples that have a large percentage of fresh groundmass glass and may yield meaningful ages from the early part of the spectrum. Type 3 spectra are obtained from samples with minimal clay alteration and where >30% of the total K resides in groundmass plagioclase. The central flat portion of the spectrum is a good measure of the age and reflects primarily the outgassing of plagioclase high K rims. Type 4 spectra are produced by samples that invariably have some amount of clay alteration which hold a significant fraction of the total K budget. Provided a sufficiently large percentage (>30%) of the total K is held in groundmass glass, and sufficient care is taken to isolate this gas fraction during incremental heating, the central mini-plateau at the top of the hump-shaped Type 4 spectra may provide a reasonably good estimate of the age. Type 5 spectra are produced by samples that are more severely altered and that were low K to begin with, such that nearly all the K resides in very fine-grained aggregates of secondary clays, zeolites, and perhaps some residual glass. These samples are usually quite quenched (i.e., originally had a large fraction of glass), and that glass is now mostly altered. In such samples, severe recoil and argon loss compounded by large Ca corrections conspire to yield strongly hump shaped spectra with no concordant ages, such that the only interpretation that can usually be made is that the top of the hump likely represents a minimum age for the sample.

Taken together, these observations suggest that acceptable ages can be obtained from groundmass separates of reasonably fresh mafic volcanic rocks provided more than at least ~30% of the total K resides in plagioclase or sanidine. Progressively better data quality and higher precisions are obtained as the overall K-content, crystallinity and grain size of the groundmass increases and the amount of secondary clay/zeolite alteration after glass decreases. The very best results, significantly better than those obtained from associated plagioclase phenocrysts, are obtained from alkaline basalts with fresh holocrystalline groundmasses.

6. Results

6.1. Sample Types

The igneous rocks that were dated in this study range from basalt to granite, but most are mafic to intermediate volcanic rocks (Table 1; Figures 2 and 3; Mortimer & Patriat, 2016). Primary igneous textures are generally well-preserved, and feldspar and pyroxene are generally fresh, but olivine is pervasively iddingsitized and groundmass glass commonly exhibits some degree of secondary alteration (Supporting Information S5). For detailed treatment of the geochemical and isotopic composition, igneous petrogenesis, and additional petrographic details of the VESPA rocks see Agranier et al. (2023) and geochemical data at https://doi.org/10.17882/90050.

Using trace element concentrations and isotopic ratios Agranier et al. (2023) divided the VESPA lavas into three geochemical groups, based on their relative trace element concentrations, and whether they had negative, flat or positive slopes in their chondrite-normalized rare-earth element (REE) patterns: (a) depleted tholeiites (negatively sloping REE patterns); (b) transitional tholeiites (flat REE patterns); (c) enriched lavas (positively sloping REE patterns), including andesites, trachyandesites and trachytes. These three groups also form distinctive Sr, Nd, Hf, and Pb isotopic arrays (Agranier et al., 2023).

The enriched geochemical group includes 14 dated lavas, mostly basaltic trachyandesites and trachyandesites with lesser basalts and trachytes (Table 1). These lavas commonly contain plagioclase and greenish clinopyroxene phenocrysts and are commonly vesicular. Phenocrysts of biotite and/or hornblende are prominent in a few of intermediate composition (e.g., DR41Aii, DR15B, DR26Aiv). The enriched group lavas were mainly dredged from tops of seamounts and ridges on the Loyalty and Three Kings Ridges and from the NW Cook Fracture Zone scarp, in relatively shallow (∼800–2,400 m) water depths (Figures 2 and 3).

The transitional and depleted tholeiite geochemical groups include 19 dated samples. These are aphyric to porphyritic, sometimes vesicular, basalts and basaltic andesites (Table 1). Some samples with doleritic groundmass and devitrified glass mesostasis (e.g., DR25Cii, DR39C) are probably from the centers of lava flows. Others have abundant glass and may be broken pillow rinds (Mortimer & Patriat, 2016). Phenocryst and groundmass phases are primarily plagioclase and colorless clinopyroxene, though sparse olivine is present in at least one sample (DR33Ai). Depleted tholeiites were mostly dredged from 1,400 to 4,100 m water depths on fault scarps and volcanic flanks from along the Cook Fracture Zone, Cagou Trough and/or abyssal plain of the South Fiji Basin. Included in this depleted group is a rhyolite from Bougainville Guyot that was originally recorded as a chert (Collot et al., 1992).

Three dm-sized pieces of altered biotite granite porphyry were dredged from 2,400 m water depth on the western Three Kings Ridge (DR26). Normative calculations of two DR26 analyses confirm that the rock name granite is correct (Streckeisen & Le Maitre, 1979). Other rocks in the dredge included trachyandesite and altered tuffisites (Mortimer & Patriat, 2016). Plagioclase and biotite phenocrysts and a holocrystalline groundmass in the granite suggest a hypabyssal setting.

The threefold geochemical and isotopic subdivision from Agranier et al. (2023) is illustrated in Figure 5. We use this figure to further interpret the dated lavas in terms of their possible tectonic setting of eruption. The fourfold petrotectonic interpretation presented in this paper enables the dated VESPA rocks to be directly compared with earlier southwest Pacific compilations (Mortimer et al., 2007, 2021; Mortimer & Scott, 2020). The separate geochemical and petrotectonic classifications of samples are given in Table 1. The same information is presented with geochemical analyses in the main supplemental data file of Agranier et al. (2023). In Figure 5, two geochemically enriched lavas lie on the mid-ocean ridge basalt to ocean island basalt (MORB-OIB) mantle array and the rest lie well above it. The two basalts on the MORB-OIB array are DR08A and DR22A and we interpret them as intraplate alkali basalts of the kind that are found scattered across the southwest Pacific region (Mortimer & Scott, 2020). Most of the VESPA light REE-enriched lavas lie above the mantle array. Their bulk compositions are typical of high-K and shoshonitic suites similar to those found on South Fiji Basin seamounts (Mortimer et al., 1998, 2007, 2022). The DR26 granite plots with the high K-shoshonitic lavas and we regard it as a plutonic member of this same suite.

The transitional tholeiites of Agranier et al. (2023) with their flat REE patterns, also scatter along and above the MORB-OIB mantle array. They, too, can be divided into two categories but less clearly than the enriched lavas. We interpret those on or close to the mantle array as being back-arc basin-like and those well above the mantle array as having possible subduction-related arc affinity (Figure 5). There is an acknowledged large overlap in geochemistry between global arc and back-arc basin lavas (e.g., Shervais, 2022), and this is especially the case in the southwest Pacific when high-Ti Early Arc Tholeiites from Fiji and rear-arc lavas from the Colville Ridge are included (Timm et al., 2019; Todd et al., 2010). Thus, our twofold (red and blue dot symbol) interpretation of these widespread basalts and basaltic andesites is likely to be a simplification. Overall, Figure 5 confirms general subduction-influenced compositions for many VESPA tholeiites including arc, rear-arc, and back-arc basin compositions and (for the Cook Fracture Zone) possibly leaky transform magmatism.

The most depleted back-arc basin-like tholeiites were obtained at VESPA dredge site 39. DR17A is notable because it was recovered from the deepest part of the northwest Cook Fracture Zone (CFZ, 3,500 m) and is a
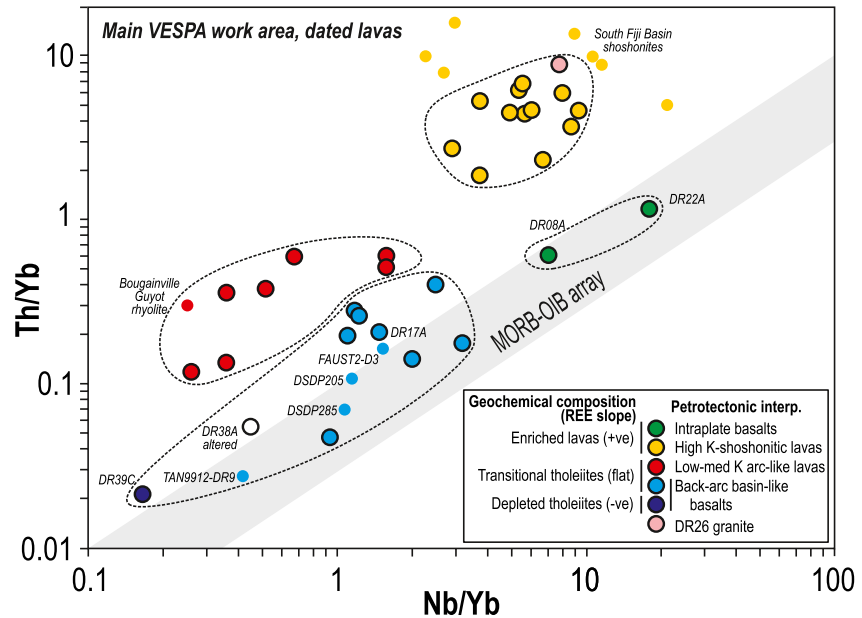
Figure 5. Dated VESPA samples plotted on a Nb/Yb versus Th/Yb diagram (Pearce, 2014). Figure shows classification in terms of geochemical and isotopic composition (Agranier et al., 2023) and interpreted petrotectonic setting of eruption (this paper). Reference data from Bernardel et al. (2002) and Mortimer et al. (2007).

clast from a tectonic breccia in which surfaces have a chloritic polish and slickensides; it is the only sample to contain a structural overprint from the CFZ. Shown for comparison in Figure 5 are other back-arc basin basalts from pre-VESPA sampling in the area of Figures 1–3: the FAUST2-D3 and TAN9912-DR9 dredges, and core from DSDP (Deep Sea Drilling Project) Sites 205 and 285 (Bernardel et al., 2002; Mortimer et al., 2007).

6.2. Ar/Ar Ages

Excellent to acceptable Ar/Ar ages were obtained from most VESPA samples. A summary of the preferred Ar/Ar age for each of the 33 dated samples is presented in Table 1, and associated age spectra are shown in Figure 6. A tabulated summary of results for all 49 dated mineral and groundmass separates is given in Supporting Information S5 and all raw data and spectra in Supporting Information S6. The methods used to obtain reported ages and age uncertainties vary. For samples that yield straightforward plateaus, where well over 50% of the ^{39}Ar is released in consecutive steps that are concordant (i.e., lie within 2σ analytical uncertainty of each other), we follow the widely accepted convention (e.g., McDougall & Harrison, 1999) of calculating a weighted mean plateau age (WMPA), with each step weighted according to its analytical uncertainty, and calculate an uncertainty in the age (2σ, 95% confidence) from the weighted mean uncertainty of all steps used in the calculation. For spectra where there are analytically concordant adjacent steps that represent less than 50% of the gas released, and for samples where there are no consecutive concordant steps, but 30%–80% of the age spectrum still define a visually flattish segment, we calculate a weighted mean age. For calculating errors for these "non-plateau" samples, we followed Fleck et al. (2014) in multiplying the propagated errors by the square root of the mean square of weighted deviates (MSWD) in cases where MSWD >1.

Having described our interpretive approach to groundmass argon spectra in terms of five types (Figure 4), we now present the VESPA ^{40}Ar/^{39}Ar results in terms of four quality ranks (A–D) based on a qualitative assessment of our overall confidence in the assigned age and uncertainty for each sample (Table 1, Figure 6). In cases where multiple phases from the same sample were analyzed, the quality rank for samples typically is based on whichever phase yielded the better result. In some cases, reinforcing results from multiple phases (e.g., plagioclase and groundmass) might, together, raise the overall rank of that sample. Quality rank A, B, and C samples all yielded ^{40}Ar/^{39}Ar ages that are acceptable and useful but have generally increasing age uncertainties. Quality rank D samples typically yielded age spectra that were so disturbed and/or had such vanishingly low K contents and K/Ca ratios that our age assignments and their uncertainties are more akin to educated guesses. A summary of the results from each group is as follows.
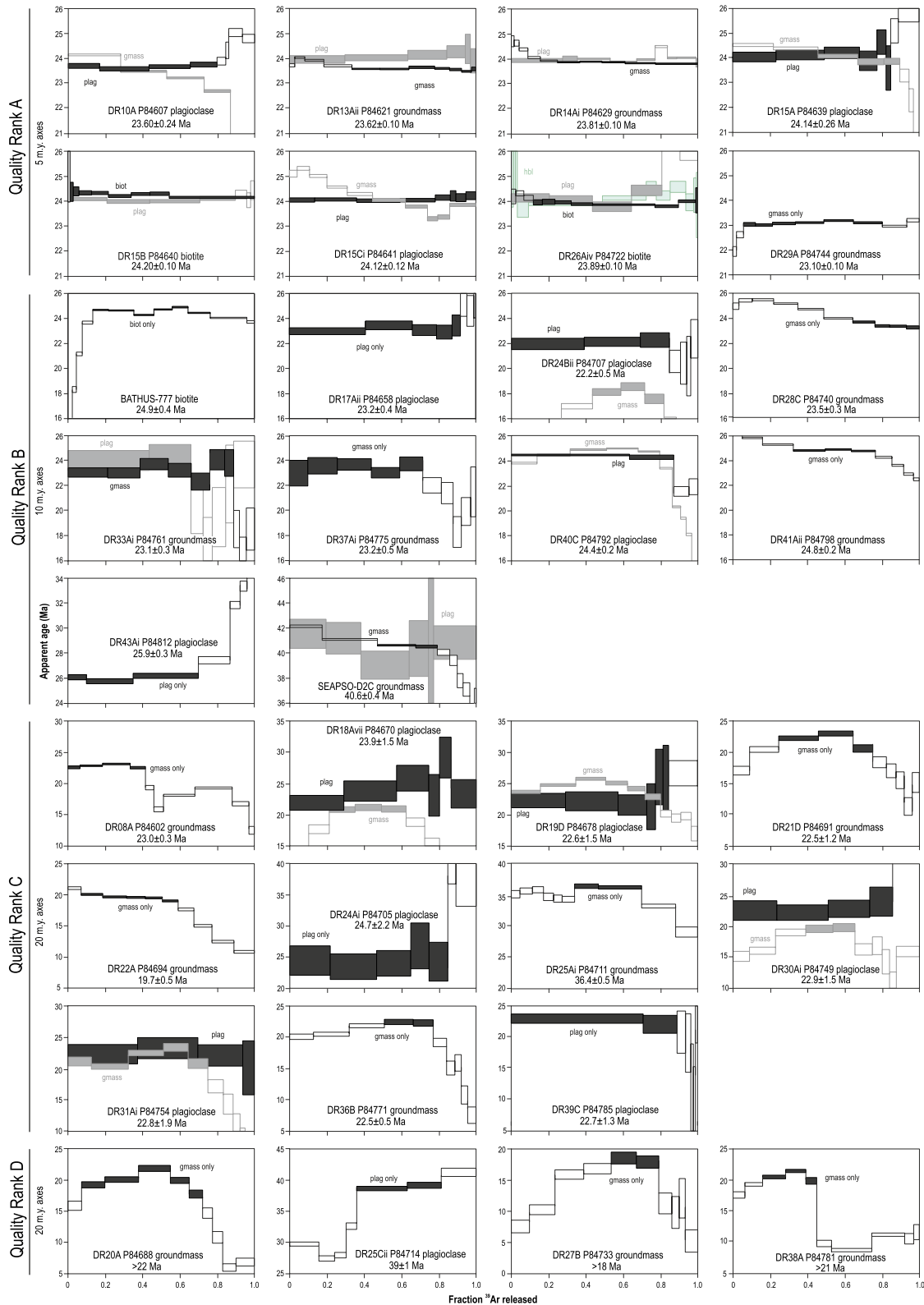
Figure 6. Ar/Ar degassing age spectra for all 33 VESPA rock samples grouped according to quality of interpreted age for the best dated separate (A = highest, D = lowest). Note vertical scale of 5 m.y. for A samples, 10 m.y. for B samples, and 20 m.y. for C and D samples. Filled boxes indicate steps used to interpret age of sample. Height of boxes is ±1σ but labeled ages and ages used in text are ±2σ.

QUALITY RANK A samples yielded the most precise Ar/Ar ages (Table 1, top two rows of Figure 6, Supporting Information S5). These are mainly intermediate to silicic volcanic rocks and the assigned age was obtained from either a phenocryst phase (biotite, plagioclase, or hornblende) or a fresh, mostly crystalline, and relatively high-K groundmass, or both. They all belong to the enriched, high K-shoshonitic group identified above and have whole rock $K_2O > 1.2$ wt%. Quality Rank A samples are the freshest, least-altered rocks in the sample set. Groundmass samples of this group yield mainly Type 1 spectra. Multiple phases were dated from all but one of the samples, and consistently gave ages that were well within analytical uncertainty of each other and of the integrated total fusion age (Figure 6, Supporting Information S5 and S6). WMPAs were calculated from 65% to 100% of the gas released and had high (65%–98%) radiogenic yields. Plagioclase phenocrysts have K/Ca = 0.05–0.10 and groundmass separates K/Ca = 0.1–2.0. Even though some bulk groundmass analyses have only moderate K/Ca, most contain late interstitial sanidine which dominates the spectrum behavior (e.g., Figure 4a). All the sample ages of Quality Rank A are closely clustered at approximately 24 Ma with uncertainties of ±0.10–0.26 Ma.

QUALITY RANK B samples also gave precise Ar/Ar ages (Table 1, rows 3–5 of Figure 6), but with somewhat less precise analytical uncertainty. These samples comprise six basalts, two basaltic andesites, a basaltic trachyandesite, and a rhyolite from which we dated seven groundmass separates, six plagioclase separates, and one biotite separate. Geochemically, both enriched and transitional igneous suites are represented. Whole rock K_2O contents vary from 0.3 to 2.5 wt%. Groundmass/plagioclase pairs were dated for four of these samples, with more precise ages obtained by groundmass for two and plagioclase for two. All age pairs agree except for P84671 the groundmass of which displays extensive argon loss. Plagioclase phenocryst K/Ca ratios were somewhat lower (0.01–0.04) than Quality Rank A samples but yielded reasonably flat spectra with well-defined WMPA from 65% to 100% of the gas released. Groundmass separates produced mainly Type 1 and 3 spectra. Despite having low K_2O (Agranier et al., 2023), some of the basalts are doleritic and their holocrystalline groundmasses are plagioclase-rich and amenable to dating (Figure 4). Overall, Quality Rank B samples have slightly more secondary alteration than Quality Rank A, especially as clay minerals replace groundmass glass. Six out of 10 samples have plateaus that meet statistical criteria of McDougall and Harrison (1999). The Quality Rank B samples are 26–22 Ma in age except for the geographically distant SEAPSO sample which gave ages of 40.6 ± 0.4 Ma (groundmass) and 41.3 ± 1.2 Ma (plagioclase). This makes it one of the oldest Eocene arc lavas with one of the highest precision ages thus far obtained from the entire southwest Pacific.

QUALITY RANK C samples include nine basalts, one basaltic andesite and one basaltic trachyandesite (Table 1, rows 6–8 of Figure 6). All lack K-rich phenocrysts. Whole rock K_2O ranges from 0.1 to 1.1 wt% and includes both enriched and depleted suites (Agranier et al., 2023), but no high K-shoshonitic lavas. Interpreted ages are based on five groundmass separates from aphyric lavas, two plagioclase separates from samples with groundmass that was too altered to date, and four samples with plagioclase-groundmass pairs. Groundmass age spectra are mostly of Type 4 and 5, with one each of Type 2 and 3. Most yielded interpretable (but low precision) ages from the flattish central parts of spectra, based on <50% of the gas released. The K/Ca ratios of groundmass separates is highly variable (0.02–0.8), and most of the complexity in the spectra reflects varying degrees of recoil and argon associated with the presence of appreciable glass and/or clay alteration, as discussed in Section 5 above. Plagioclase phenocrysts yielded fairly flat (Type 1) spectra for 80%–100% of the gas released but have large uncertainties due to the small signal sizes, low K contents, very low K/Ca ratios (0.002–0.005) and associated large Ca corrections. Uncertainties in the ages of Quality Rank C samples are significantly higher than Rank A and B, ranging from ±0.3–2.2 Ma, (mostly ± 1.2–1.5 Ma), reflecting their lower K contents and greater degree of alteration.

QUALITY RANK D samples (bottom row of Figure 6) are the most mineralogically altered and have abundant clays and zeolites in groundmass. Three samples are depleted olivine basalts that lack plagioclase phenocrysts, the other is a clay-altered hyaloclastite breccia (DR38A). Whole rock K_2O of the four samples is 0.2–0.8 wt% and groundmass K/Ca is notably low—generally <0.05. Most results likely do not represent primary crystallization ages but we include them in this paper because they are an instructive end member in the range of Ar/Ar behavior of submarine basalts. At best, only minimum ages can be inferred from most of these strongly hump-shaped Type 5 groundmass spectra, which arise from substantial hydrothermal alteration and recoil issues. An imprecise age of 39 ± 1 Ma from the doleritic groundmass plagioclase of DR25Cii is given by two concordant steps which make up 45% of the gas, but this age is highly uncertain given the overall complexity of the spectrum.

The most notable aspect of our VESPA Ar/Ar dating is that 25 of the 33 samples have estimated ages that are tightly clustered between 25 and 22 Ma that is, they straddle the Oligocene-Miocene boundary (Figure 7). This
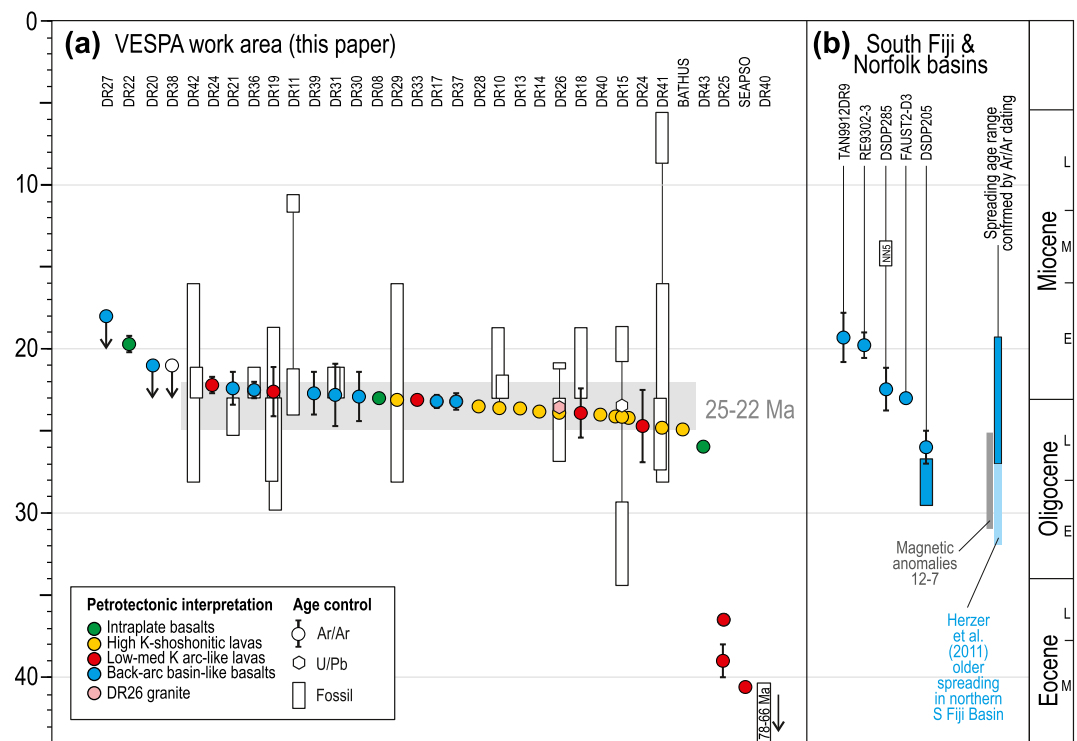
Figure 7. (a) Newly reported ages for VESPA igneous rocks (this paper) ordered left to right from youngest to oldest. Circle and hexagon symbols are Ar/Ar and U/Pb ages, white rectangles are supporting microfossil ages on samples from the same dredge. (b) Previously established direct dating of South Fiji and Norfolk basin crust (Bernardel et al., 2002; Edwards, 1973; Mortimer et al., 1998, 2007, 2014). These, and the VESPA ages, confirm a younger spreading age range than that based on magnetic anomalies (Davey, 1982; Malahoff et al., 1982; Sdrolias et al., 2003; Watts et al., 1977). In both panels, where circles have no error bars, the 2σ age error lies within the size of the symbol.

is irrespective of their geochemical composition, map location, or dredge depth. Four samples gave ages that are slightly younger than this range, but three of them are minima and thus their eruptive ages could also be in the range 25–22 Ma. One DR43 lava—from the Norfolk Ridge—gave an age of 25.9 Ma. The remaining three lavas in our new Ar/Ar data set have ages between 41 and 36 Ma (Middle to Late Eocene); one of these is from Bougainville Guyot which, like DR43, is outside the main VESPA work area (Figures 1–3). Within the 25–22 Ma cluster, the enriched high-K lavas are, overall, slightly older than the more depleted lavas. The geological significance and tectonic implications of the results for the wider southwest Pacific are discussed at more length in Section 7.

6.3. U-Pb Zircon Geochronology

Zircons from two samples, biotite granite porphyry DR26Fiii and sandstone DR15Cii, were dated by the U-Pb method (Figure 8). Cathodoluminescence images and raw U-Pb isotope data tables are given in Supporting Information S5. Zircons extracted from VESPA DR26Fiii are up to 600×150 μm in size, euhedral, and show oscillatory igneous zoning. Of the 30 zircons dated, 16 were <10% discordant and are plotted in Figure 8b. All but the youngest define a single age population of 23.6 ± 0.3 Ma which we interpret as the intrusion age of the granite porphyry. This is within error of the 23.9 ± 0.1 Ma Ar/Ar age of enriched lava DR26Aiv from the same dredge. Abundant biotite phenocrysts in the DR26Fiii granite porphyry suggests that it is related to the biotite-bearing "enriched" (shoshonitic) group of lavas, as does its whole rock geochemistry (Agranier et al., 2023). Despite targeting zircon cores, no older ages, for example, suggestive of Mesozoic basement, were found. This implies either an absence of Zealandia continental crust under the DR26 dredge site, that granite magmagenesis didn't involve continental crust, or that zircons were fully reset or recrystallized such that evidence of any older inheritance was not preserved.
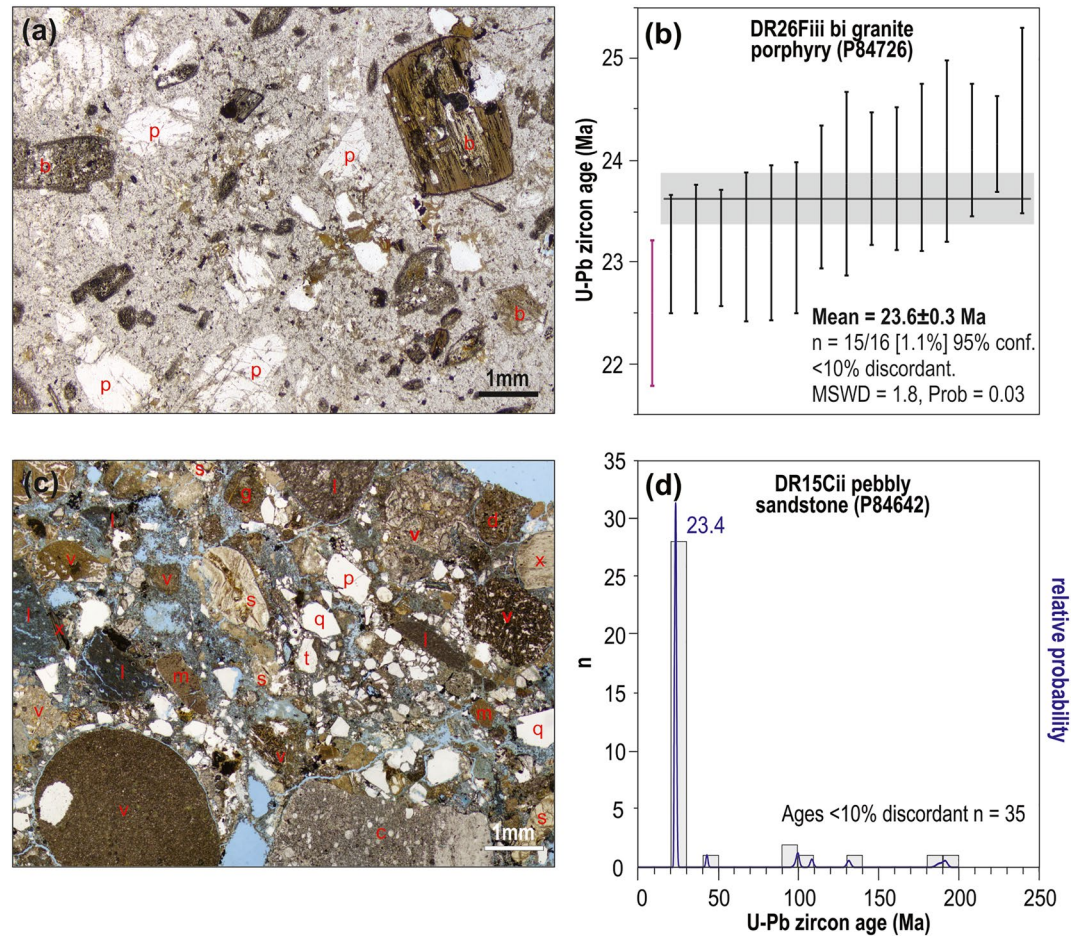
Figure 8. Thin section images of samples dated by U-Pb zircon methods, and their age plots (a) DR26Fiii biotite granite porphyry, plane-polarized light. p, plagioclase; b, biotite phenocrysts. The holocrystalline groundmass contains alkali feldspar and quartz. (b) DR26Fiii individual concordant $^{238}U/^{206}Pb$ grain ages placed left to right from youngest to oldest. Fifteen grains are used to calculate an age of 23.6 ± 0.3 Ma. (c) DR15Cii polymict pebbly sandstone, plane-polarized light. c, chert; d, dolerite; g, gabbro; l, limestone; m, mudstone; p, plagioclase; q, quartz; s, serpentinite; v, volcanic rock; x, exsolved clinopyroxene. The section was made with blue-dyed epoxy which occupies void spaces and cracks; clay minerals have been plucked during section production. (d) DR15Cii individual $^{238}U/^{206}Pb$ zircon ages shown in a histogram. Relative probability function (blue line) shows that most zircons define a single population with age 23.4 Ma.

VESPA dredge 15 contained c. 600 kg of clastic sedimentary rock pieces. Lithologic contacts between conglomerate, pebbly sandstone, sandstone, siltstone, and mudstone rock types in many of the dredged pieces suggests that we sampled across a well-bedded sedimentary formation (Mortimer & Patriat, 2016). The main rock type is a polymict bouldery to pebbly matrix-rich sandstone with a few thin (<5 cm) medium-grained sandstone to mudstone beds (VESPA DR15Cii). The cobble- and boulder-sized clasts are all volcanic (DR15A, B, Ci; Table 1) and one very-well rounded, 10 cm diameter cobble of silicified limestone (DR15F) was noted. Granule-sized clasts in a thin section of DR15Cii (Figure 8c) are mostly varitextured lava and mudstone, with subordinate clasts of serpentinite, chert, marble, limestone, gabbro with saussuritized feldspars, dolerite, variolitic basalt, amphibole gneiss, and discrete grains of clear monocrystalline quartz, clear (volcanic) feldspar, exsolved (plutonic) clinopyroxene, and pale tremolitic amphibole. Thus, the sandstone appears to have a threefold provenance: chilled volcanic rocks, limestones, and an altered ophiolite sequence. The most obvious candidate for an ophiolitic source area is an offshore correlative of the Peridotite and Poya nappes of the New Caledonia Subduction-Obduction Assemblage (Maurizot, Robineau, et al., 2020). Such rocks have been traced to near the Cook Fracture Zone (Patriat et al., 2018).

Zircons extracted from the sandstone matrix of DR15Cii are up to 400 × 100 μm in size, euhedral, and show oscillatory igneous zoning. None are rounded. Of the 87 zircons dated, 35 were <10% discordant and are plotted

in Figure 8d. The majority (28 grains) define a peak at 23.4 ± 0.3 Ma that is very close to the 24.2–24.1 Ma Ar/Ar ages of three dated volcanic clasts from the same sandstone. Older zircon grain ages are 43, 99, 100, 108, 131, 188, and 192 Ma. The Cretaceous and Jurassic ages match those of detrital zircons in New Caledonia and New Zealand Eastern Province basement rocks (e.g., Adams et al., 2009; Campbell et al., 2018). As such they indicate erosion of similar basement terranes, which are expected to lie along the north-eastern edge of Zealandia.

6.4. Micropaleontology

A total of 63 limestone and mudstone samples from 23 VESPA dredges were processed and examined for their microfossil content. Of these, 32 yielded no fauna or gave non-determinate ages, and nine gave Plio-Pleistocene ages. The remaining 22 samples from 13 dredge sites yielded pre-Pliocene ages summarized in Table 3 and Figure 7 (these exclude the Norfolk Ridge seamount samples already reported in Mortimer et al. [2021]). Full details of the micropaleontology of the VESPA samples are presented in Supporting Information S8 (Crundwell et al., 2016).

Ten micropaleontologically dated mudstone and limestone samples are in contact with volcanic or volcaniclastic material for example, as crack infills or micrite breccia matrix (Table 3), and 12 micropaleontologically dated samples are from pieces of sedimentary rock. The overlapping or younger micropaleontological ages, though inherently of lower precision, generally support the Ar/Ar ages of the lavas in the same dredge (Figure 7). The ages of two samples are especially noteworthy. (a) The oldest dated VESPA mudstone is the Late Cretaceous DR40F from the northern tip of the Three Kings Ridge at c. 3,700 m water depth. (b) Forams from the mud matrix of bouldery to pebbly sandstone DR15Cii (Figure 8c) indicate a stratigraphic age of Early Miocene (Otaian: 20.9–18.7 Ma). Reworked Early Oligocene (34.6–29.2 Ma) fauna are present in D15Cii, and plausibly are from the limestone clasts. As noted above, lava clasts from the same sandstone are 24.2–24.1 Ma (Figure 7) and detrital zircons from the sandstone are mainly c. 23 Ma with some older Mesozoic grains (Figure 8d).

Paleo-water depths for the VESPA samples (Table 3) are usually minima and poorly constrained due a paucity of calibrated benthic foraminifera depth markers. However, most interpreted paleo-depths broadly match the water depths at which the samples have been dredged. Shelf restricted taxa and faunas in two samples (DR26Gi and DR42Ci) indicate these sample sites have subsided in situ since deposition or the samples have slumped off bathymetric highs and have been redeposited in deeper water.

7. Discussion

7.1. Best Ar/Ar Practice and Interpretation

In this study, we have improved knowledge of the interpretation of complex Ar/Ar spectra of groundmass separates from mafic volcanic rocks. This has been achieved by integrating detailed petrographic, microprobe, and geochronological data. What has emerged is a much better understanding of the causes of the different argon spectrum shapes and some insights on how best to interpret these disturbed (non-ideal) age spectra to assign a reasonable age. When trying to obtain $^{40}Ar/^{39}Ar$ ages from groundmass separates of mafic volcanic rocks, we recommend the following:

- If possible, sample holocrystalline interiors of thick lava flows rather than chilled margins.
- Conduct careful petrographic examination to identify both phenocryst and groundmass phases and to enable crushing of the sample to a size range that ensures capture of pure groundmass particles and inclusion-free portions of plagioclase phenocrysts, typically 100–250 μm.
- Perform several hours of heavy-duty ultrasonic cleaning in repeated baths of deionized water to remove as much secondary clay as possible.
- Date both groundmass and phenocrystic plagioclase separates. This allows independent verification of the assessed age.
- Conduct quantitative microprobe analyses and create element concentration maps of representative groundmass areas on a polished thin section. This will reveal where potassium is residing in the groundmass and how it is apportioned between different phases.
- In degassing experiments of groundmass separates, distribute the gas evenly between at least 9–10 temperature steps during incremental heating. The gas released between the 600–1100°C steps is the most informative.

Table 3
Summary of Pre-Pliocene VESPA Microfossil Ages

Dredge #	Rock	Key taxa	Fossil zone	Stage	Age range (Ma)	Paleo-depth (m)
DR10B	Hard, silicified limestone with ashy parts	*Zeaglobigerina brazieri, Z. woodi-connecta, Globoquadrina dehiscens*	N4a–N4b	Mid Lw	23.0–21.7	>200
DR10D	Silicified and bored lst hardground	*G. dehiscens, Z. woodi*	N4a–N6	Late Lw–Po	23.0–18.7	>600
DR11A	Soft bioturbated siltstone	*Paragloborotella mayeri, Z. nepenthes*	N14	Late Sw–early Tt	11.6–10.6	>1,000
DR11B	Weakly indurated, bored chalky limestone	*Fohsella kugleri.* Absence of *globoconellids*	N4a	Late Lw–early Po	23.0–21.1	>600
DR15Cii	Hard, yellowish-gray, polymict pebbly sandstone	*Mixed age fauna* (1) *S. angiporoides* and no *Globigerinatheka* index. (2) *G. dehicens, G. incognita, C. dissimilis, Z. woodi, Z. connecta*	P17–P20 and N5–N6	Early Lw and Po	34.6–29.18 20.9–18.7	>200
DR18C	Hard, white chalky limestone from crack in breccia	*G. dehicens, Z. woodi, Z. connecta, P. semivera.* Absence of *globoconellids*	N4a–N7	Late Lw–mid Po	23.0–18.7	>600
DR19Jii	Soft, pale yellowish-green mudstone	*Catapsydrax dissimilis, Globorotaloides testarugosa, Z. woodi, Z. connecta*	N4a–N7	Late Lw–mid Po	23.0–18.7	>1,000
DR19Jiii	Soft, pale gray calcareous mudstone	*C. dissimilis, Neogloboquadrina nana, G. testarugosa.* Absence of *G. dehiscens, Z. euapertura, Subbotina, Globigerinatheka*	P22	Late Lwh–Ld	28.1–23.0	>200
DR19K	Soft, gray, chalky lst cavity fill in DR19H breccia	*Z. euapertura.* Absence of *Subbotina, Z. woodi, Z. connecta, G. deshiscens*	P20–P22	Lwh–early Lw	29.8–23.0	>600
DR21G	Soft white matrix to hyaloclastite breccia	*G. dehiscens, Z. euapertura, Z. woodi, C. dissimilis*	P22	Early Lw	25.2–23.0	>1,000?
DR26Gi	Hard, micrite cement to volcanic breccia	*F. kugleri, Globigerina altipertura.* Absence of *globoconellids*	N5–N7	Early Po	21.1–20.9	<200?
DR26Gii	Similar description to DR26Gi: separate piece	*G. dehiscens, C. dissimillis, G. tripartita, Z. euapertura*	P22	Ld–early Lw	26.9–23.0	>200
DR29C	Hard limestone matrix to volcanic conglomerate	Possible benthic *Cribrorotalia amatissima*	na	Late Olig.–E. Mio.	28.1–16.0	>200
DR31Bi	Soft yellowish-gray calcareous mudstone	*F. kugleri, Z. connecta*	N4a–N4b	Late Lw–early Po	23.0–21.1	>1,000
DR31C	Soft calcareous mudstone	*F. kugleri, Z. connecta, Z. woodi*	N4a–N4b	Late Lw–early Po	23.0–21.1	>1,000
DR36E	Soft, pale yellowish-gray calcareous mudstone	*F. kugleri, Z woodi, Z. connecta, G dehiscnes, Catapsydrax dissimilis*	N4a–N4b	Late Lw–early Po	23.0–21.1	>1,000
DR40F	Radiolarian-bearing pale olive-gray silty mudstone	*Dictyomitra andersoni, Lithocampe wharanui, Theocapsomma erdnussa.* Absence of Paleocene species	RK9	Late Camp.–Maas.	78–66	na
DR41Di	Hard, micrite cement to volcanic breccia	*G. tripartita, P. semivera*	P22–N7	Late Olig.–E. Mio.	27.3–17.3	>1,000?
DR41Dii	Micrite fracture fill in volcaniclastic sst	*C. diissimillis, G. tripartita, G. testarugosa, Z. euapertura-woodi.* Absence of *G. dehiscens*	P22	Ld–early Lw	27.3–23.0	>800
DR41Ei	Cemented, bored foram limestone	*G. conglobatus, G. miotumida*	N17B–N18	Mid Tt–Tk	8.6–5.5	>200?

Table 3
Continued

Dredge #	Rock	Key taxa	Fossil zone	Stage	Age range (Ma)	Paleo-depth (m)
DR42Ci	Hard, bioclastic calcarenite (bryozoan packstone)	*C. amatissima*	na	Ld—Sw	28.1–16.0	<100
DR42D	Soft, light olive-gray calcareous mudstone	*F. kugleri*	N4a–N4b	Late Lw	23.0–21.1	>1,500

Note. See Supporting Information S8 (Crundwell et al., 2016) for complete micropaleontological report. Stages from Raine et al. (2015). Taxa are foraminifera except for sample DR40F (radiolarians).

- Interpret age spectra using their shapes, associated K/Ca spectra, degassing behavior, and acquired knowledge of the phases present and K distribution. A reasonable age interpretation can then often be made even for very complicated spectra, where only a small fraction of the gas is used in the age determination.

We recognize that many of these procedures, especially the first three, are now routinely followed by investigators obtaining $^{40}Ar/^{39}Ar$ ages from mafic lavas (e.g., Calvert & Lanphere, 2006; Fleck et al., 2014; Leonard et al., 2017), but most of these investigations dated very fresh, relatively young onland basalts where subaerial exposures provide the luxury of selecting the best material possible to date. Here we emphasize the importance of thoroughly investigating the detailed petrography and mineral/glass chemistry of the different groundmass phases for samples that are glassy and/or altered, in order to establish precisely what phases are contributing to the radiogenic argon budget and to better interpret complex age spectra that might otherwise be deemed uninterpretable.

7.2. Geology of the Loyalty Ridge-Three Kings Ridge Area

The Loyalty-Three Kings Ridge area was formerly one of the least-known parts of the southwest Pacific. Because of this paper, it is now one of the most densely sampled and dated. Our new dating results are shown on local seismic profile cross sections (Figure 9) and on a regional southwest Pacific map (Figure 10). The northern and southern cross sections of Figure 9 have the main axes of the Loyalty Ridge and Three Kings Ridge aligned by restoring c. 250 km of Cook Fracture Zone (CFZ) movement between them (Crawford et al., 2003; Herzer et al., 2011). Such a restoration also suggests a pre-CFZ alignment—and therefore correlation—of other features such as South Loyalty Basin = Three Kings Terrace, Félicité Ridge = un-named basement high of the western Three Kings Terrace and, more speculatively, Kwênyii Basin = Philip Trough. The distinctly deep Cagou Trough, which cuts the Philip Trough structure (Figure 3a; DiCaprio et al., 2009; Sdrolias et al., 2004) does not appear to have an obvious counterpart north of the Cook Fracture Zone. Two disadvantages of rock dredging are that sampling is done along a line rather than at a point, and that individual blocks potentially have moved downslope from their in situ locations. Nonetheless, the cross sections of Figure 9 reveal that, with a few (slumped?) exceptions, the high K-shoshonitic lavas are always found on bathymetric highs (800–2,400 m water depth), and most back-arc basin-like lavas are found in bathymetric lows including the Cook Fracture Zone (3,500–4,200 m water depth). The dredging of Eocene as opposed to Oligocene-Miocene arc lavas at DR25, along with the granite at DR26, can be explained by their low structural-stratigraphic position exhumed in the footwall block of a major normal fault on the eastern side of the Cagou Trough.

The most significant result arising from our dating work reported in this paper is recognition of a voluminous and exceptionally widespread pulse of latest Oligocene to earliest Miocene (25–22 Ma) igneous activity within, north, and south of the Cook Fracture Zone between latitudes 25°S and 22°S (Figures 9–11). An episode of Middle to Late Eocene volcanism also seems to be documented but is less well-constrained because of fewer dated rocks both in the VESPA work area and elsewhere. The Middle to Late Eocene DR25 lavas were recovered from the unnamed basement high of the western Three Kings Terrace that is, west of the main Loyalty-Three Kings ridge axis *sensu stricto*. Early Oligocene DR15C limestones were also recovered in a relatively westerly location from the Félicité Ridge. The DR40 Late Cretaceous mudstone, DR15 detrital zircons of Mesozoic age, and DR15 detrital serpentinite suggest that the ultimate geological basement to the ridges in the VESPA work area could be continental Zealandia.
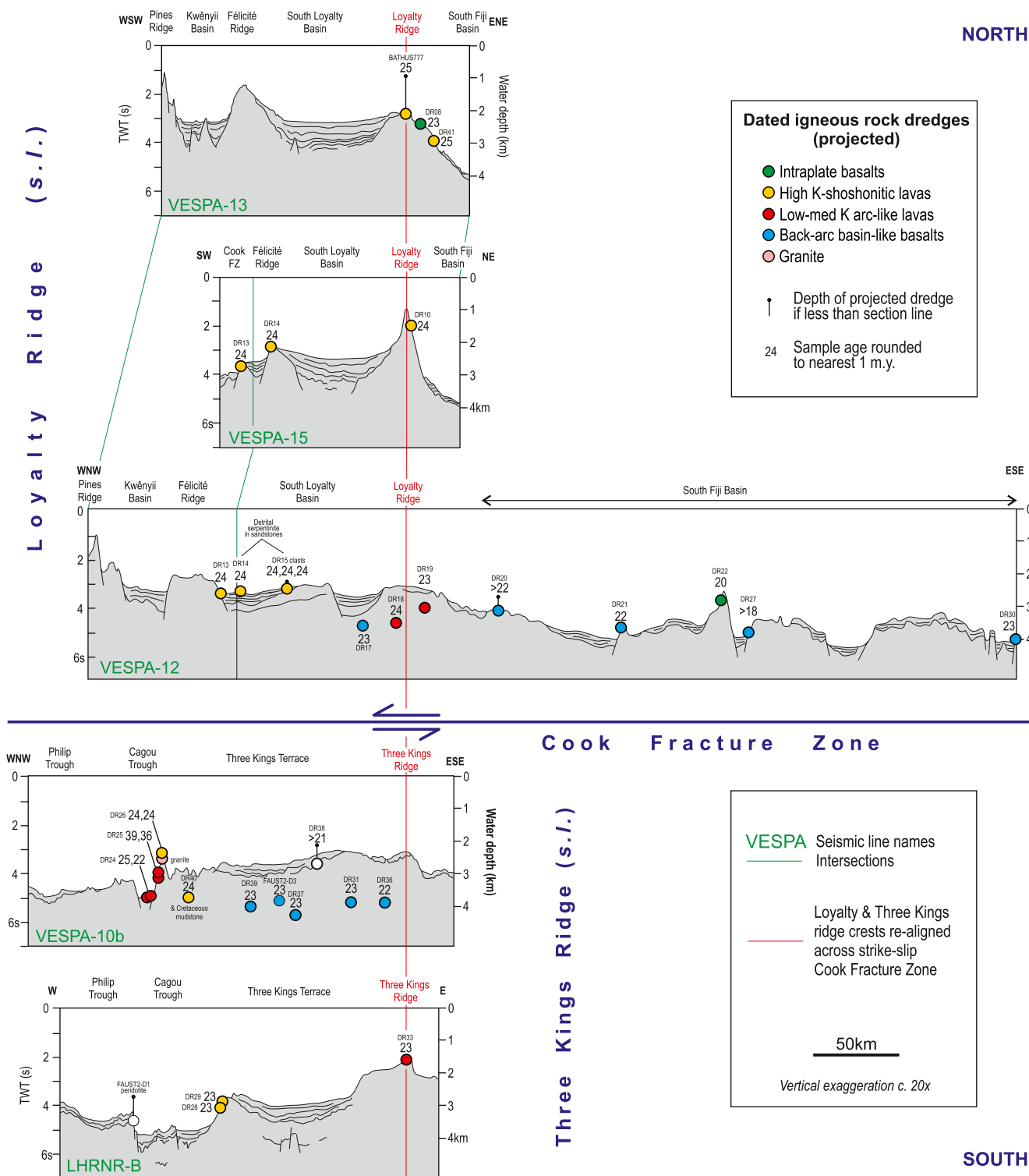
Figure 9. Age and compositional data for VESPA igneous rocks plotted on five lightly interpreted seismic reflection profiles (Mortimer & Patriat, 2016). See Figure 2a for profile locations. Profiles are ordered from north (top of page) to south (bottom of page) and have been positioned left-to right so that the crests of the Loyalty Ridge (*sensu stricto*) and Three Kings Ridge (*sensu stricto*) coincide. Such a restoration of the c. 250 km sinistral offset on the Cook Fracture Zone better shows the relative positions of the Loyalty and Three Kings Ridge VESPA dredge sites. Line LHRNR-B is from Ramsay et al. (1997). TWT = two-way travel time. Patriat et al. (2018) gave interpretations of VESPA seismic lines north of these.
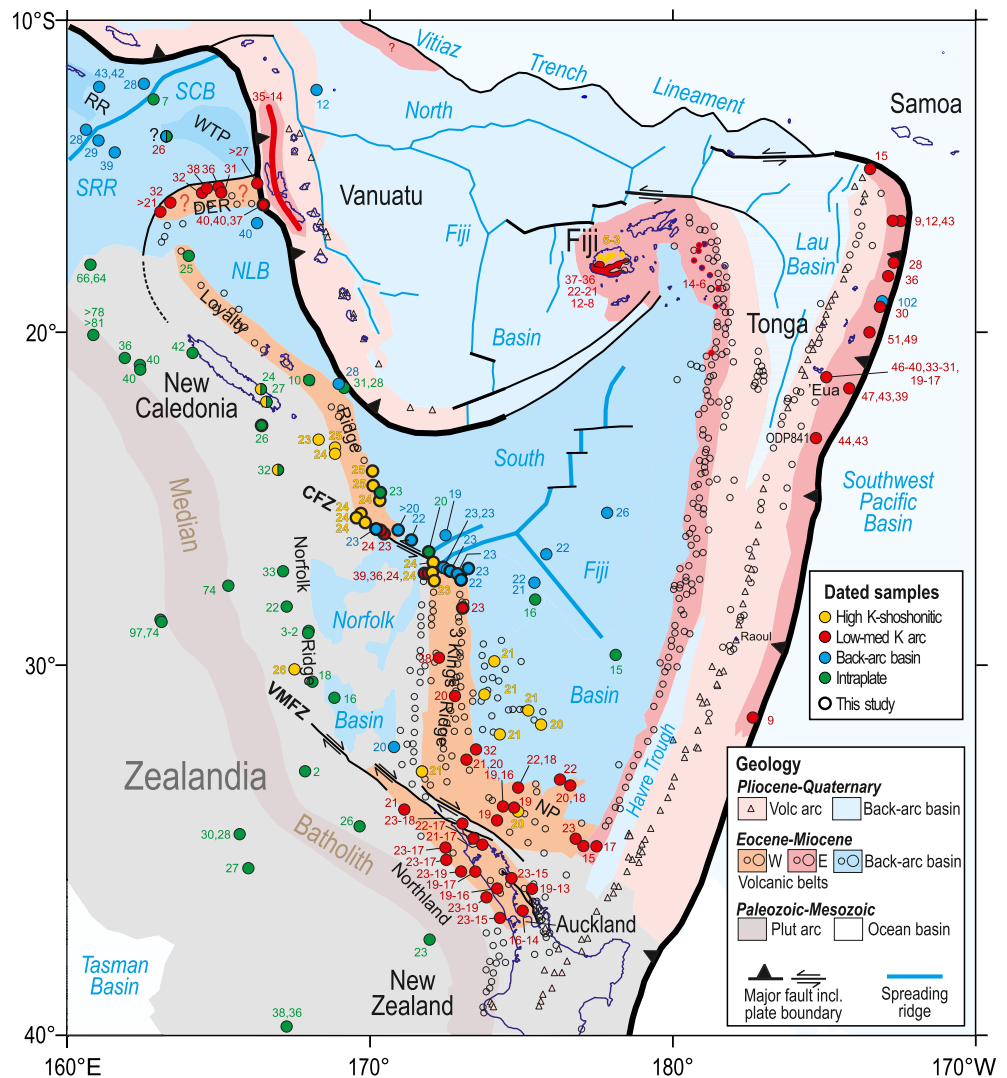
Figure 10. Map showing Eocene to Middle Miocene subduction-related volcanic rocks of the southwest Pacific. A disrupted >3,000 km-long western belt (orange, the topic of this paper) lies between New Zealand in the south and the D'Entrecasteaux Ridge (DER) in the north and has been broken and bent by the opening of the South Fiji, Norfolk, North Loyalty, and D'Entrecasteaux Basins (medium blue color). A disrupted eastern belt (dark pink) is present in and/or near Tonga, Fiji, Vanuatu and, speculatively, along the Vitiaz Trench Lineament. The figure is a simple geological-lithological map that does not attempt to explain the complexity of how the belts formed as composite and superimposed arc segments. Mesozoic and Pliocene-Quaternary arcs shown in pale brown and pale pink colors. RR, Rennell Ridge; WTP, West Torres Plateau; SCB, Santa Cruz Basin; SRR, South Rennell Ridge; NLB, North Loyalty Basin; CFZ, Cook Fracture Zone; NP, Northland Plateau; VMFZ, Vening Meinesz Fault Zone. Offshore data from this study and Pelletier and Auzende (1996), Mortimer et al. (1998, 2007, 2010, 2014, 2015, 2018, 2021, 2022), Ballance et al. (1999), Herzer et al. (2011), Meffre et al. (2012), Seton et al. (2016), and MacLeod et al. (2017). Onland data from Gill and Whelan (1989), Rodda (1994), Hayward et al. (2001), Paquette and Cluzel (2007), Stratford (2009), Shane et al. (2010), Rickard and Williams (2013), Buys et al. (2014), and Marien et al. (2022).

The results greatly add to the picture of southwest Pacific arc volcanism on the Loyalty and Three Kings Ridges. Previously, knowledge of their geology was based on a meager data set of a 37.5 Ma boninite (un-named basement high of the western Three Kings Terrace), 32 Ma andesite (Northland Plateau) and a 20 Ma andesite (Three Kings Ridge) (Figure 10; Bernardel et al., 2002; Mortimer et al., 1998, 2007). Prior to VESPA, the only dated samples from the Loyalty Ridge were intraplate basalts of 10 Ma age on the island of Maré (latitude 21°S; Maurizot & LaFoy, 2003) and a 25 Ma lava from a seamount at 19°S (Mortimer et al., 2018). Our work conclusively shows that the Loyalty Ridge and the formerly contiguous Three Kings Ridge (*sensu stricto*) are mainly composed of 25–22 Ma Late Oligocene-Early Miocene lavas, with subordinate 39–36 Ma Eocene lavas.
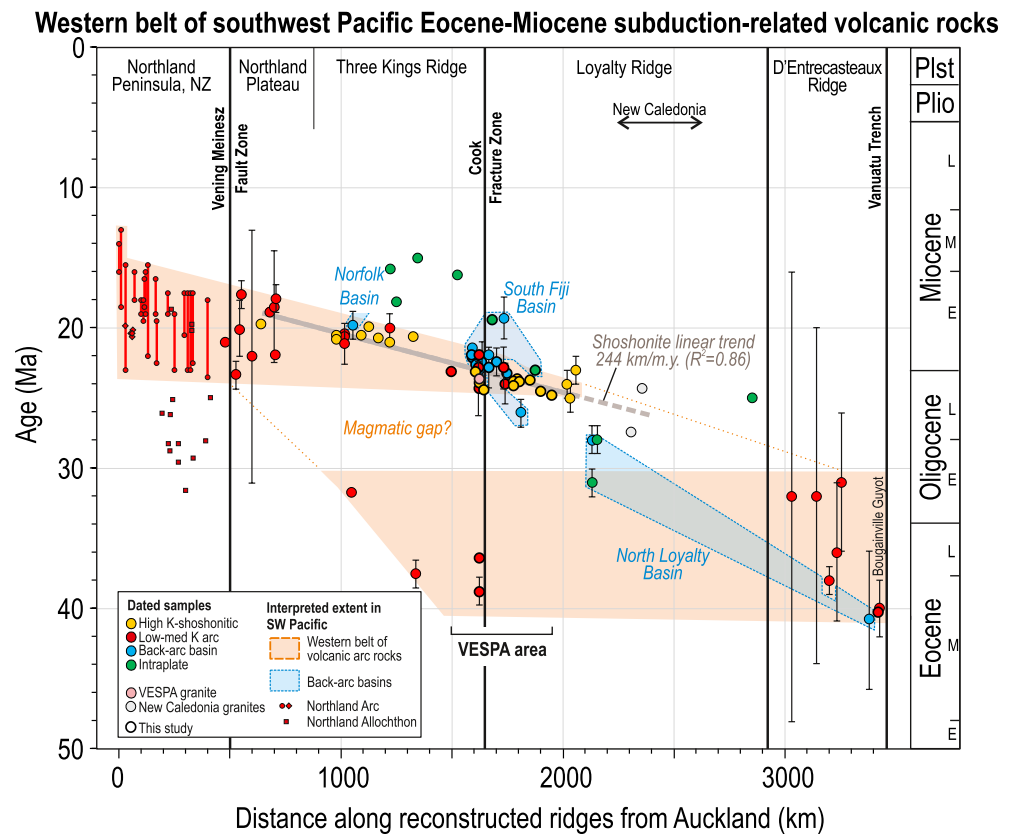
Figure 11. Age profile along the >3,000 km-long western volcanic belt between New Zealand and the D'Entrecasteaux Ridge. *X*-axis position has been calculated as along-strike distance from Auckland, taking into account offset along the Vening Meinesz Fault Zone and Cook Fracture Zone. Ages of individual dredge samples have two sigma error bars; ages for Northland Arc volcanoes are ranges. The VESPA samples, either side of the Cook Fracture Zone, fill a critical data gap. On available information, both the age of inception and the age of cessation of currently interpreted arc volcanism apparently decrease to the south. The ages of the immediately adjacent basins follow a similar trend. Data from same sources as Figure 10.

7.3. Age of South Fiji Basin Spreading

For many years the age of spreading of the abyssal South Fiji Basin was cited as 31–25 Ma (Oligocene) based on an interpretation of magnetic anomalies 12–7 (Davey, 1982; Malahoff et al., 1982; Sdrolias et al., 2003; Watts et al., 1977). This age is shown as the gray bar in Figure 7b. In contrast, Ar/Ar dating of five back-arc basin basalts by Bernardel et al. (2002) and Mortimer et al. (2007), including at DSDP Sites 205 and 285 (Figure 7b), suggested a younger age for spreading, and Herzer et al. (2011) showed that the magnetic reversal patterns could also be fitted to Early Miocene anomalies 9–6B. Our VESPA expedition increased the number of direct age determinations on South Fiji and Norfolk back-arc basin basalts from five to 14.

The oldest confirmed age of South Fiji Basin spreading is provided by a high-quality Ar/Ar plagioclase age of 26 ± 1 Ma, from DSDP Site 205 (Mortimer et al., 2007). DSDP Site 205 is situated toward the eastern edge of the basin (Figures 1 and 10) in what are interpreted as older, but not the oldest, spreading anomalies (Herzer et al., 2011). Most of the VESPA back-arc basin basalt ages from near the Cook Fracture Zone (CFZ) for example, DR21, DR30, DR36, TAN9912-DR9 are much younger than 26 Ma (Figure 7a) and, sensibly, lie closer to the fossil Central Minerva-Cook spreading axis (Figures 3a and 10). Five back-arc basin basalts dredged from the Cook Fracture Zone are all c. 23 Ma in age and probably represent leaky transform volcanism between South Fiji and Norfolk Basin spreading centers. Abyssal hill fabric and the negligible change in water depth between the basins indicate crust of similar age on either side of the CFZ (Herzer et al., 2011). A reasonably precise minimum age on CFZ movement and, therefore on South Fiji—Norfolk Basin spreading, is provided by the DR22A seamount dated at 19.7 ± 0.5 Ma. This elongate intraplate volcano protrudes 8 km across the CFZ fault trace

and therefore seals it (Figure 3a). The 14 Ar/Ar ages and their error envelopes thus support a 27–19 Ma age for South Fiji Basin spreading rather than c. 31–25 Ma based on magnetic anomalies (Figure 7b). However, there is space in the northern South Fiji Basin for crust of pre-27 Ma age (Herzer et al., 2011). Late Oligocene-Early Miocene extensional tectonics was not just confined to the South Fiji and Norfolk Basins. Horsts, graben, and tilted terraces are present in adjacent arc and continental crust, notably as South Loyalty and Kwênyii Basins, and Philip and Cagou Troughs (Figures 2, 3, and 9; Patriat et al., 2018).

7.4. Western Belt of Remnant Arcs

The broader context of Oligocene-Miocene subduction-related lavas on the southern Loyalty Ridge and northern Three Kings Ridge is illustrated in Figures 10 and 11. Based on age and composition, Mortimer et al. (2007) made the case that the now spatially separate Miocene volcanic arcs of onland Northland, the Northland Plateau and the Three Kings Ridge were formerly contiguous and had been split apart by the dextral Vening Meinesz Fault Zone (Figure 10). There is now sufficient geological evidence for us to postulate the existence of a >3,000 km long Cenozoic volcanic belt between Northland New Zealand and Bougainville Guyot (Figures 1, 10, and 11). Tectonic continuity along similarly long southwest Pacific baselines had been previously postulated in syntheses by Lapouille (1977), Launay et al. (1982), and Recy and Dupont (1982) based on bathymetric and magnetic expression, and by Crawford et al. (2003), Schellart et al. (2006), Whattam et al. (2008), and McCarthy et al. (2022) using bathymetry and scattered ophiolite occurrences to infer locations of associated subduction zones. Our work is the first to confirm the extent of a belt of Cenozoic volcanic rocks as shown in Figure 10. We are most confident about its continuity between Northland and the Loyalty Ridge and less confident about it on the D'Entrecasteaux Ridge.

As shown in Figures 10 and 11, the age range of subduction-related lavas in the main VESPA work area is 39–22 Ma (this study); that on the D'Entrecasteaux Ridge, including Bougainville Guyot, is 40–31 Ma but with large errors (Mortimer et al., 2014; this study). We have not attempted to document volcanic arc rocks farther west toward Papua New Guinea (but see Whattam et al., 2008). The main gap in our knowledge remains the northern Loyalty Ridge. There is an along-strike distance of ~1,300 km between our VESPA Loyalty Ridge work area and the next Cenozoic arc-related volcano on the D'Entrecasteaux Ridge with only intraplate basalt sites in-between (Figures 10 and 11).

Most of the >3,000 km Northland-Loyalty-D'Entrecasteaux volcanic belt likely formed where it currently sits—along the north-eastern continent-ocean boundary of Zealandia. It represents the westernmost manifestation of southwest Pacific Cenozoic subduction-related volcanism. The belt's rearward arc position is supported by the relatively high Nb/Yb relative to Th/Yb of the shoshonites; the VESPA lavas are not volcanic front lavas which would be rich in fluid mobile elements and poor in high field strength elements. Existing ages and our new ages from the western volcanic belt possibly suggest two pulses of subduction-related volcanism c. 40–30 Ma and 25–16 Ma (orange areas in Figure 11), separated by a 30–25 Ma hiatus. In other words, lavas from two episodes of arc volcanism seem to be superimposed in the one belt of volcanic rocks. The small number of Eocene samples so far obtained from the southwest Pacific is a natural consequence of most sampling being by rock dredging. Despite our efforts on the VESPA voyage to sample the lower part of fault scarps, dredge-based sampling will always be biased to the youngest eruptive episodes, particularly given low erosion rates in submarine settings. The c. 40 Ma start of arc volcanism over the >3,000 km length of the western volcanic belt can be correlated with regional Eocene deformation which has been interpreted to record southwest-dipping Pacific subduction initiation (Sutherland et al., 2017, 2020; Stratford et al., 2022; see also van de Lagemaat et al., 2022). The <40 Ma arc footprint of the western volcanic belt postdates 56–40 Ma events in New Caledonia including ophiolite sole amphibolite formation, dikes with arc chemistry and blueschist facies metamorphism (Maurizot, Cluzel, et al., 2020). These older events have been linked to initiation and jamming of a north-east dipping subduction zone culminating in Peridotite Nappe obduction (Crawford et al., 2003; Maurizot, Cluzel, et al., 2020; Meffre et al., 2012; Schellart et al., 2006; Whattam, 2009), and which may be unrelated to <40 Ma tectonic geometries.

We see some analogies of the development of our western and eastern volcanic belts split by the South Fiji Basin, with the situation in the Cenozoic western Pacific. There, the remnant western Kyushu-Palau arc was split from the eastern Izu-Bonin-Mariana arc by the Shikoku and Parece Vela Basins; shoshonites are also present in the Parece Vela Basin (Ishizuka et al., 2010, 2011). Pacific-Australian convergence vectors in north-east Zealandia changed little in the interval 45–0 Ma, apart from a slight acceleration and small change in azimuth at c. 27 Ma

(Bache et al., 2012). Possible causes of the apparent pulse of volcanic arc activity at c. 25–22 Ma could include changing nature of the subducting slab, maturation of the subduction zone, onset of intra-arc extension facilitating magmatic flux, backarc basin opening, and/or collisional tectonics.

7.5. Eastern Belt of Arcs

The back-arc basins of the southwest Pacific attest to substantial trench rollback (Karig, 1971). Eocene and Miocene arcs were variously split by back-arc, intra-arc, and fore-arc rifting mechanisms (Figure 6 of Stern [2006]), some rifts developed into wide back-arc basins. The back-arc basin opening shifted segments of Eocene, Oligocene, and/or Miocene arc lavas laterally from the edge of Zealandia to locations in Vanuatu, Fiji, Tonga, and the Tonga forearc (Figure 10; Bloomer et al., 1994; Duncan et al., 1985; Hathway & Colley, 1994; Macfarlane et al., 1988; Marien et al., 2022; Meffre et al., 2012; Rickard & Williams, 2013; Rodda, 1994; Timm et al., 2019) and, more speculatively, the Vitiaz Trench Lineament and Kermadec forearc (Bassett et al., 2016; Pelletier & Auzende, 1996). Under sampled Eocene to Miocene arc rocks in the eastern belt now form the basement to the more prominent and better-studied Pliocene-Quaternary arcs (Figure 10). Since the Eocene, active arc volcanism has always lain close to the east-migrating Pacific trench (and, since the Late Miocene subduction polarity flip, the southward migrating Vanuatu Trench).

7.6. Southwest Pacific Shoshonitic Volcanism

High K-shoshonitic lavas are not only present on the crests of Loyalty and Three Kings Ridges but are also present elsewhere along and across strike (Figure 10). Their ages are very well-constrained due to their high K contents. In the VESPA work area, they are consistently 24–23 Ma in age. To the south, 21-20 Ma shoshonite lavas have been dredged from six seamounts in the southern South Fiji Basin and as pebbles on the Three Kings Terrace (Mortimer et al., 1998, 2007, 2022). To the north, two shoshonitic lavas and a pebble, dated at 25–23 Ma, have been dredged from the Félicité Ridge and Pines Ridge south of New Caledonia (Mortimer et al., 2014). By analogy with rift-related Pliocene shoshonites in Fiji (Gill & Whelan, 1989) and arc extension elsewhere (Ishizuka et al., 2010), the Oligocene-Miocene shoshonites in and near the VESPA work area have been related to rapid arc rifting. The scenario is that the shoshonites erupted in and near a waning western volcanic belt above a deep Pacific slab as the South Fiji Basin opened rapidly and the Pacific trench migrated rapidly east (Agranier et al., 2023; Mortimer et al., 2007, 2021). This widespread southwest Pacific Early Miocene rift setting fits with the relatively high Nb/Yb of the shoshonites (Figure 5), subtle indications of Miocene extension in and near New Caledonia (Chardon & Chevillotte, 2006; Lagabrielle et al., 2005), Oligocene-Miocene extension in the Kwênyii and South Loyalty Basins (Patriat et al., 2018), our interpretation of the Cagou Trough as an extensional graben (Figure 9), and Miocene movement on the Vening Meinesz Fracture Zone (Herzer et al., 2009).

Using the arc distance from Auckland as a baseline (Figure 10), a regression line through the shoshonite ages reveals a southward-younging trend of ~240 km/m.y. within a relatively short ~5 m.y. interval (Figure 11). This may represent a southward-younging trend in the rifting—a long-baseline "unzipping" of the basins (Herzer et al., 2011). Interestingly, the shoshonite regression line in Figure 11 projects toward the age and position of the two granite stocks in New Caledonia (the only known Oligocene igneous rocks there). Mortimer et al. (2014) argued that they were petrogenetically related to the Félicité Ridge and Pines Ridge shoshonites and were related to incipient post-obduction extension (cf., Cluzel et al. [2005] and Sevin et al. [2020] who offered an alternative explanation connecting the granites to east-dipping Oligocene subduction).

8. Conclusions

This paper has presented the results of detailed Ar/Ar dating of rocks from the 2015 VESPA cruise, supported by U/Pb and micropaleontological dating. The study area of the Three Kings Ridge, Loyalty Ridge, and nearby South Fiji Basin has now gone from one of the least sampled parts of the southwest Pacific to one of the most densely sampled. Challenges in $^{40}Ar/^{39}Ar$ dating of submarine basalts can be addressed by appropriate sample preparation techniques, thorough petrographic and microprobe characterization of groundmass phases, carefully designed incremental heating experiments, and by dating groundmass and mineral pairs whenever possible. These protocols allow informed interpretation of "disturbed" Ar/Ar age spectra in terms of varying amounts of argon loss, reactor induced recoil, and excess argon. An understanding of these complexities and especially of

how K is distributed between various reservoirs allows for meaningful age assignments even from samples that lack statistical plateaus and might otherwise be viewed as undatable and/or uninterpretable.

Our work has demonstrated the existence of a previously unsuspected major pulse of 25–22 Ma magmatism on and in the vicinity of the Three Kings Ridge, Loyalty Ridge, and Cook Fracture Zone, southwest Pacific Ocean. Key findings include: (a) evidence for Middle-Late Eocene arc volcanism along and near the northeast edge of the Zealandia continent, with lavas as old as 40–36 Ma on the D'Entrecasteaux and western Three Kings Ridges, but still only ~23 Ma in Northland New Zealand; (b) during and after their formation, arcs were split by intra-arc and cross-arc rifting accompanied by back-arc basin opening. This kept active eastern arc segments close to the Pacific trench and slab, and stranded western remnant arc segments (the topic of this paper) in a >3,000 km-long belt between New Zealand and the D'Entrecasteaux Ridge; (c) these magmatic and tectonic changes can be explained in terms of <40 Ma Pacific trench rollback to the east dragging the active arc with it and creating widespread extension and eruption of shoshonites in the back-arc regions. Eastward trench rollback was accompanied by an overall north to south "unzipping" of Eocene-Early Miocene back-arc basins with time (back-arc basins are older and wider in the north). (d) the large number and broad geographic distribution of samples that yield ages between 25 and 22 Ma suggests that this was a particularly prolific time of rear arc-related volcanism—part of a regional latest Oligocene to earliest Miocene magmatic flareup. The results of this paper provide valuable data for future work on the rates and causes of Cenozoic tectonic change in the southwest Pacific Ocean.

Conflict of Interest

The authors declare no conflicts of interest relevant to this study.

Data Availability Statement

All eight Supporting Information files for this paper are available on the SEANOE website at https://doi.org/10.17882/89740. The whole rock geochemical analyses of VESPA rocks are available in a data file at https://doi.org/10.17882/90050. Additional information about the VESPA cruise, including the Mortimer and Patriat (2016) voyage report, can be found at https://doi.org/10.17600/15001100.

References

Adams, C. J., Cluzel, D., & Griffin, W. L. (2009). Detrital-zircon ages and geochemistry of sedimentary rocks in basement Mesozoic terranes and their cover rocks in New Caledonia, and provenances at the Eastern Gondwanaland margin. *Australian Journal of Earth Sciences*, *56*(8), 1023–1047. https://doi.org/10.1080/08120090903246162

Agranier, A., Patriat, M., Mortimer, N., Collot, J., Etienne, S., Durance, P. M. J., & Gans, P. B. (2023). Subduction-related volcanism on the Loyalty and Three Kings ridges, SW Pacific: A precursor to the Tonga-Kermadec arc. *Lithos*, *436–437*, 106981. https://doi.org/10.1016/j.lithos.2022.106981

Bache, F., Sutherland, R., Stagpoole, V. M., Herzer, R. H., Collot, J., & Rouillard, P. (2012). Stratigraphy of the southern Norfolk Ridge and the Reinga Basin: A record of initiation of Tonga-Kermadec–Northland subduction in the southwest Pacific. *Earth and Planetary Science Letters*, *321–322*, 41–53. https://doi.org/10.1016/j.epsl.2011.12.041

Ballance, P. F., Ablaev, A. G., Pushchin, I., Pletnev, S. P., Birylina, M. G., Itaya, T., et al. (1999). Morphology and history of the Kermadec trench–arc–backarc basin–remnant arc system at 30 to 32°S: Geophysical profile, microfossil and K–Ar data. *Marine Geology*, *159*(1–4), 35–62. https://doi.org/10.1016/s0025-3227(98)00206-0

Bassett, D., Kopp, J., Sutherland, R., Henrys, S., Watts, A. B., Timm, C., et al. (2016). Crustal structure of the Kermadec arc from MANGO seismic refraction profiles. *Journal of Geophysical Research: Solid Earth*, *121*(10), 7514–7546. https://doi.org/10.1002/2016jb013194

Bernardel, G., Carson, L. J., Meffre, S., Symonds, P. A., & Mauffret, A. (2002). Geological and morphological framework of the Norfolk Ridge to Three Kings Ridge region. *Geoscience Australia Record*, *2002*(08).

Bloomer, S. H., Ewart, A., Hergt, J. M., & Bryan, W. B. (1994). Geochemistry and origin of igneous rocks from the outer Tonga forearc (Site 841). *Proceedings of the Ocean Drilling Program, Scientific Results*, *135*, 625–646.

Buys, J., Spandler, C., Holm, R. J., & Richards, S. W. (2014). Remnants of ancient Australia in Vanuatu: Implications for crustal evolution in island arcs and tectonic development of the southwest Pacific. *Geology*, *42*(11), 939–942. https://doi.org/10.1130/g36155.1

Calvert, A. T., & Lanphere, M. A. (2006). Argon geochronology of Kilauea's early submarine history. *Journal of Volcanology and Geothermal Research*, *151*(1–3), 1–18. https://doi.org/10.1016/j.jvolgeores.2005.07.023

Campbell, M. J., Shaanan, U., Rosenbaum, G., Allen, C. M., Cluzel, D., & Maurizot, P. (2018). Permian rifting and isolation of New Caledonia: Evidence from detrital zircon geochronology. *Gondwana Research*, *60*, 54–68. https://doi.org/10.1016/j.gr.2018.04.004

Chardon, D., & Chevillotte, V. (2006). Morphotectonic evolution of the New Caledonia ridge (Pacific Southwest) from post-obduction tectono-sedimentary record. *Tectonophysics*, *420*(3–4), 473–491. https://doi.org/10.1016/j.tecto.2006.04.004

Clowes, C. D., Crampton, J. S., Bland, K. J., Collins, K. S., Prebble, J. G., Raine, J. I., et al. (2021). The New Zealand Fossil Record File: A unique database of biological history. *New Zealand Journal of Geology and Geophysics*, *64*(1), 62–71. https://doi.org/10.1080/00288306.2020.1799827

Cluzel, D., Bosch, D., Paquette, J. L., Lemennicier, Y., Montjoie, P., & Menot, R. P. (2005). Late Oligocene post-obduction granitoids of New Caledonia: A case for reactivated subduction and slab break-off. *Island Arc*, *14*(3), 254–271. https://doi.org/10.1111/j.1440-1738.2005.00470.x

Collot, J., Patriat, M., Sutherland, R., Williams, S., Cluzel, D., Seton, M., et al. (2020). Geodynamics of the SW Pacific: A brief review and relations with New Caledonian geology. *Geological Society, London, Memoir*, *51*(1), 13–26. https://doi.org/10.1144/m51-2018-5

Collot, J.-Y., Lallemand, S., Pelletier, B., Eissen, J.-P., Glaçon, G., Fisher, M. A., et al. (1992). Geology of the D'Entrecasteaux-New Hebrides Arc collision zone: Results from a deep submersible survey. *Tectonophysics*, *212*(3–4), 213–241. https://doi.org/10.1016/0040-1951(92)90292-e

Crawford, A. J. (2004). Voyage summary Southern Surveyor 01/2003. Unpublished CSIRO report updated 22/04/04. Retrieved from https://www.marine.csiro.au/data/reporting/get_file.cfm?eov_pub_id=866

Crawford, A. J., Meffre, S., & Symonds, P. A. (2003). 120 to 0 Ma tectonic evolution of the southwest Pacific and analogous geological evolution of the 600 to 220 Ma Tasman Fold Belt System. *Geological Society of Australia Special Publication*, *22*, 377–397.

Crundwell, M. P., Morgans, H. E. G., & Hollis, C. J. (2016). Micropaleontological report on dredge samples collected during the 2015 VESPA (Volcanic Evolution of South Pacific Arcs) expedition. *GNS Science Internal Report, 2016/22*.

Dalrymple, G. B., & Lanphere, M. A. (1974). $^{40}Ar/^{39}Ar$ age spectra of some undisturbed terrestrial samples. *Geochimica et Cosmochimica Acta*, *38*(5), 715–738. https://doi.org/10.1016/0016-7037(74)90146-x

Davey, F. J. (1982). The structure of the South Fiji Basin. *Tectonophysics*, *87*(1–4), 185–241. https://doi.org/10.1016/0040-1951(82)90227-x

DiCaprio, L., Müller, R. D., Gurnis, M., & Goncharov, A. (2009). Linking active margin dynamics to overriding plate deformation: Synthesizing geophysical images with geological data from the Norfolk Basin. *Geochemistry, Geophysics, Geosystems*, *10*(1), Q01004. https://doi.org/10.1029/2008GC002222

Dickin, A. P. (2005). *Radiogenic isotope geology* (2nd ed.). Cambridge University Press.

Duncan, R. A., Vallier, T. L., & Falvey, D. A. (1985). Volcanic episodes at 'Eua, Tonga Islands'. In D. W. Scholl & T. L. Vallier (Eds.), *Geology and offshore Resources of Pacific island arcs—Tonga region*, *Circum-Pacific Council for Energy and Mineral Resources Earth Science Series* (Vol. 2, pp. 281–290). Circum-Pacific Council for Energy and Mineral Resources.

Edwards, A. R. (1973). Calcareous nannofossils from the southwest Pacific, Deep Sea Drilling Project, Leg 21. *Initial Reports of the Deep Sea Drilling Project*, *21*, 641–691.

Fleck, R. J., Hagstrum, J. T., Calvert, A. T., Evarts, R. C., & Conrey, R. M. (2014). $^{40}Ar/^{39}Ar$ geochronology, paleomagnetism, and evolution of the Boring volcanic field, Oregon and Washington, USA. *Geosphere*, *10*(6), 1283–1314. https://doi.org/10.1130/ges00985.1

Gans, P. B. (1997). Large-magnitude Oligo-Miocene extension in southern Sonora: Implications for the tectonic evolution of northwest Mexico. *Tectonics*, *16*(3), 388–408. https://doi.org/10.1029/97tc00496

GEBCO Compilation Group. (2019). The GEBCO_2019 Grid—A continuous terrain model of the global oceans and land. https://doi.org/10.5285/836f016a-33be-6ddc-e053-6c86abc0788e

Gill, J., Hoernle, K., Todd, E., Hauff, F., Werner, R., Timm, C., et al. (2021). Basalt geochemistry and mantle flow during early backarc basin evolution: Havre Trough and Kermadec Arc, southwest Pacific. *Geochemistry, Geophysics, Geosystems*, *22*(2), e2020GC009339. https://doi.org/10.1029/2020GC009339

Gill, J., & Whelan, P. (1989). Early rifting of an oceanic island arc (Fiji) produced shoshonitic to tholeiitic basalts. *Journal of Geophysical Research*, *94*(B4), 4561–4578. https://doi.org/10.1029/jb094ib04p04561

Gurnis, M., Hall, C., & Lavier, L. (2004). Evolving force balance during incipient subduction. *Geochemistry, Geophysics, Geosystems*, *5*(7), Q07001. https://doi.org/10.1029/2003GC000681

Hall, R. E. (2002). Cenozoic geological and plate tectonic evolution of SE Asia and the SW Pacific: Computer-based reconstructions, model and animations. *Journal of Asian Earth Sciences*, *20*(4), 353–431. https://doi.org/10.1016/s1367-9120(01)00069-4

Hathway, B., & Colley, H. (1994). Eocene to Miocene geology of southwest Viti Levu, Fiji. In A. J. Stevenson, R. H. Herzer, & P. F. Ballance (Eds.), *Geology and submarine resources of the Tonga-Lau-Fiji region*, *SOPAC Technical Bulletin* (Vol. 8, pp. 153–169).

Hayward, B. W., Black, P. M., Smith, I. E. M., Ballance, P. F., Itaya, T., Doi, M., et al. (2001). K-Ar ages of early Miocene arc-type volcanoes in northern New Zealand. *New Zealand Journal of Geology and Geophysics*, *44*(2), 285–311. https://doi.org/10.1080/00288306.2001.9514939

Herzer, R. H., Barker, D. H. N., Roest, W. R., & Mortimer, N. (2011). Oligocene-Miocene spreading history of the northern South Fiji Basin and implications for the evolution of the New Zealand plate boundary. *Geochemistry, Geophysics, Geosystems*, *12*(2), Q02004. https://doi.org/10.1029/2010GC003291

Herzer, R. H., Davy, B., Mortimer, N., Quilty, P. G., Chaproniere, G. C. H., Jones, C., et al. (2009). Seismic stratigraphy and structure of the Northland Plateau and the development of the Vening Meinesz transform margin, SW Pacific Ocean. *Marine Geophysical Researches*, *30*(1), 21–60. https://doi.org/10.1007/s11001-009-9065-1

Isaac, M. J., Herzer, R. H., Brook, F. J., & Hayward, B. W. (1994). *Cretaceous and Cenozoic sedimentary basins of Northland, New Zealand* (Vol. 8). Institute of Geological & Nuclear Sciences Monograph.

Ishizuka, O., Taylor, R. N., Yuasa, M., & Ohara, Y. (2011). Making and breaking an island arc: A new perspective from the Oligocene Kyushu-Palau arc, Philippine Sea. *Geochemistry, Geophysics, Geosystems*, *12*(5), Q05005. https://doi.org/10.1029/2010GC003440

Ishizuka, O., Yuasa, M., Tamura, Y., Shukuno, H., Stern, R. J., Naka, J., et al. (2010). Migrating shoshonitic magmatism tracks Izu–Bonin–Mariana intra-oceanic arc rift propagation. *Earth and Planetary Science Letters*, *294*(1–2), 111–122. https://doi.org/10.1016/j.epsl.2010.03.016

Iwata, N., & Kaneoka, I. (2000). On the relationships between the ^{40}Ar-^{39}Ar dating results and the conditions of basaltic samples. *Geochemical Journal*, *34*(4), 271–281. https://doi.org/10.2343/geochemj.34.271

Karig, D. E. (1971). Origin and development of marginal basins in the western Pacific. *Journal of Geophysical Research*, *76*(11), 2542–2561. https://doi.org/10.1029/jb076i011p02542

Lagabrielle, Y., Maurizot, P., Lafoy, Y., Cabioch, G., Pelletier, B., Régnier, M., et al. (2005). Post-Eocene extensional tectonics in Southern New Caledonia (SW Pacific): Insights from onshore fault analysis and offshore seismic data. *Tectonophysics*, *403*(1–4), 1–28. https://doi.org/10.1016/j.tecto.2005.02.014

Lapouille, A. (1977). Magnetic surveys over the rises and basins in the South-West Pacific. In *International Symposium on Geodynamic in South-West Pacific, Nouméa (New Caledonia), 1977* (pp. 15–28).

Launay, J., Dupont, J., & Lapouille, A. (1982). The Three Kings Ridge and Norfolk Basin (Southwest Pacific): An attempt at a structural interpretation. *South Pacific Marine Geological Notes*, *2*, 121–130.

Lawrence, M. J. F., Morgans, H. E. G., Crundwell, M. P., & Patriat, M. (2020). Carbonate rocks of offshore northern Zealandia. *New Zealand Journal of Geology and Geophysics*, *63*(1), 66–89. https://doi.org/10.1080/00288306.2019.1626745

Leonard, G. S., Calvert, A. T., Hopkins, J. L., Wilson, C. J. N., Smid, E. R., Lindsay, J. M., & Champion, D. E. (2017). High-precision $^{40}Ar/^{39}Ar$ dating of Quaternary basalts from Auckland Volcanic Field, New Zealand, with implications for eruption rates and paleomagnetic correlations. *Journal of Volcanology and Geothermal Research*, *343*, 60–74. https://doi.org/10.1016/j.jvolgeores.2017.05.033

Macfarlane, A., Carney, J. N., Crawford, A. J., & Greene, H. G. (1988). Vanuatu – A review of the onshore geology. In H. G. Greene & F. L. Wong (Eds.), *Geology and offshore resources of Pacific island arcs – Vanuatu region*, *Circum-Pacific Council for Energy and Mineral Resources Earth Science Series* (Vol. 8, pp. 45–91). Circum-Pacific Council for Energy and Mineral Resources.

MacLeod, S. J., Williams, S. E., Matthews, K. J., Müller, R. D., & Qin, X. (2017). A global review and digital database of large-scale extinct spreading centers. *Geosphere*, *13*(3), 911–949. https://doi.org/10.1130/ges01379.1

Malahoff, A., Feden, R. H., & Fleming, H. S. (1982). Magnetic anomalies and tectonic fabric of marginal basins north of New Zealand. *Journal of Geophysical Research*, *87*(B5), 4109–4125. https://doi.org/10.1029/jb087ib05p04109

Marien, C. S., Drewes-Todd, E. K., Stork, A., Todd, E., Gill, J. B., Hoffmann, J. E., et al. (2022). Juvenile continental crust evolution in a modern oceanic arc setting: Petrogenesis of Cenozoic felsic plutons in Fiji, SW Pacific. *Geochimica et Cosmochimica Acta*, *320*, 339–365. https://doi.org/10.1016/j.gca.2021.11.033

Mauffret, A., Symonds, P., Benkhelil, J., Bernardel, G., Buchanan, C., D'Acremont, E., et al. (2001). *Collaborative Australia/France multibeam seafloor mapping survey–Norfolk Ridge to Three Kings Ridge region: FAUST-2, preliminary results*. Geoscience Australia Record 2001/27.

Maurizot, P., Cluzel, D., Patriat, M., Collot, J., Iseppi, M., Lesimple, S., et al. (2020). The Eocene-Oligocene subduction-obduction complex of New Caledonia. *Geological Society, London, Memoir*, *51*(1), 93–30. https://doi.org/10.1144/m51-2018-70

Maurizot, P., & LaFoy, Y. (2003). *Maré, Tiga, Walpole, Dudun et Leliogat, Iles Loyauté. Première édition. Carte géologique de la Nouvelle-Calédonie, 1:50 000*. Nouvelle-Calédonie Service des Mines et de l'Energie.

Maurizot, P., Robineau, B., Vendé-Leclerc, M., & Cluzel, D. (2020). Introduction to New Caledonia: Geology, geodynamic evolution and mineral resources. *Geological Society, London, Memoir*, *51*, 1–12.

McCarthy, A., Magri, L., Sauermilch, I., Fox, J., Seton, M., et al. (2022). The Louisiade ophiolite: A missing link in the western Pacific. *Terra Nova*, *34*(2), 146–154. https://doi.org/10.1111/ter.12578

McDougall, I., & Harrison, M. T. (1999). *Geochronology and thermochronology by the $^{40}Ar/^{39}Ar$ method* (2nd ed.). Oxford University Press.

Meffre, S., Crawford, A. J., & Quilty, P. G. (2006). Arc-continent collision forming a large island between New Caledonia and New Zealand in the Oligocene. *ASEG Extended Abstracts*, *2006*(1), 1–3. https://doi.org/10.1071/ASEG2006ab111

Meffre, S., Falloon, T. J., Crawford, A. J., Hoernle, K., Hauff, F., Duncan, R. A., et al. (2012). Basalts erupted along the Tongan fore arc during subduction initiation: Evidence from geochronology of dredged rocks from the Tonga fore arc and trench. *Geochemistry, Geophysics, Geosystems*, *13*(12), Q12003. https://doi.org/10.1029/2012GC004335

Mortimer, N., Bosch, D., Laporte-Magoni, C., Todd, E., & Gill, J. B. (2022). Sr, Nd, Hf and Pb isotope geochemistry of Early Miocene shoshonitic lavas from the South Fiji Basin: Note. *New Zealand Journal of Geology and Geophysics*, *65*(2), 374–379. https://doi.org/10.1080/00288306.2021.1876110

Mortimer, N., Campbell, H. J., Tulloch, A. J., King, P. R., Stagpoole, V. M., Wood, R. A., et al. (2017). Zealandia: Earth's hidden continent. *Geological Society of America Today*, *27*(3), 28–35. https://doi.org/10.1130/gsatg321a.1

Mortimer, N., Gans, P. B., Meffre, S., Martin, C. E., Seton, M., Williams, S., et al. (2018). Regional volcanism of northern Zealandia: Post-Gondwana breakup magmatism on an extended, submerged continent. *Geological Society, London, Special Publication*, *463*(1), 199–226. https://doi.org/10.1144/sp463.9

Mortimer, N., Gans, P. B., Palin, J. M., Herzer, R. H., Pelletier, B., & Monzier, M. (2014). Eocene and Oligocene basins and ridges of the Coral Sea-New Caledonia region: Tectonic link between Melanesia, Fiji, and Zealandia. *Tectonics*, *33*(7), 1386–1407. https://doi.org/10.1002/2014tc003598

Mortimer, N., Gans, P. B., Palin, J. M., Meffre, S., Herzer, R. H., & Skinner, D. N. B. (2010). Location and migration of Miocene–Quaternary volcanic arcs in the SW Pacific region. *Journal of Volcanology and Geothermal Research*, *190*(1–2), 1–10. https://doi.org/10.1016/j.jvolgeores.2009.02.017

Mortimer, N., Herzer, R. H., Gans, P. B., Laporte-Magoni, C., Calvert, A. T., & Bosch, D. (2007). Oligocene–Miocene tectonic evolution of the South Fiji Basin and Northland Plateau, SW Pacific Ocean: Evidence from petrology and dating of dredged rocks. *Marine Geology*, *237*(1–2), 1–24. https://doi.org/10.1016/j.margeo.2006.10.033

Mortimer, N., Herzer, R. H., Gans, P. B., Parkinson, D. L., & Seward, D. (1998). Basement geology from Three Kings Ridge to West Norfolk Ridge, southwest Pacific Ocean: Evidence from petrology, geochemistry and isotopic dating of dredge samples. *Marine Geology*, *148*(3–4), 135–162. https://doi.org/10.1016/s0025-3227(98)00007-3

Mortimer, N., & Patriat, M. (2016). VESPA cruise report. Volcanic Evolution of South Pacific Arcs. n/o L'Atalante, Nouméa – Nouméa, 22 May - 17 June 2015. *SGNC Rapport N° SGNC – 2016 (02)*. Retrieved from http://archimer.ifremer.fr/doc/00343/45408/

Mortimer, N., Patriat, M., Gans, P. B., Agranier, A., Chazot, G., Collot, J., et al. (2021). The Norfolk Ridge seamounts: Eocene–Miocene volcanoes near Zealandia's rifted continental margin. *Australian Journal of Earth Sciences*, *68*(3), 368–380. https://doi.org/10.1080/08120099.2020.1805007

Mortimer, N., & Scott, J. M. (2020). Volcanoes of Zealand and the SW Pacific. *New Zealand Journal of Geology and Geophysics*, *63*(4), 371–377. https://doi.org/10.1080/00288306.2020.1713824

Mortimer, N., Turnbull, R. E., Palin, J. M., Tulloch, A. J., Rollet, N., & Hashimoto, T. (2015). Triassic–Jurassic granites on the Lord Howe Rise, northern Zealandia. *Australian Journal of Earth Sciences*, *62*, 735–742. https://doi.org/10.1080/08120099.2015.1081984

Nauert, J., & Gans, P. B. (1994). $^{40}Ar/^{39}Ar$ geochronology of whole rock basalts: Examples from the Patsy Mine and Mt. Davis Volcanics, Eldorado Mountains, southern Nevada. *Geological Society of America Abstracts with Programs*, *26*(2), 76.

Paquette, J.-L., & Cluzel, D. (2007). U–Pb zircon dating of post-obduction volcanic-arc granitoids and a granulite-facies xenolith from New Caledonia. Inference on Southwest Pacific geodynamic models. *International Journal of Earth Sciences*, *96*(4), 613–622. https://doi.org/10.1007/s00531-006-0127-1

Patriat, M., Collot, J., Etienne, S., Poli, S., Clerc, C., Mortimer, N., et al. (2018). New Caledonia obducted peridotite nappe: Offshore extent and implications for obduction and post-obduction processes. *Tectonics*, *37*(4), 1077–1096. https://doi.org/10.1002/2017tc004722

Pearce, J. A. (2014). Immobile Element Fingerprinting of Ophiolites. *Elements*, *10*(2), 101–108. https://doi.org/10.2113/gselements.10.2.101

Pelletier, B., & Auzende, J.-M. (1996). Geometry and structure of the Vitiaz Trench Lineament (SW Pacific). *Marine Geophysical Researches*, *18*(2–4), 305–335. https://doi.org/10.1007/bf00286083

Raine, J. I., Beu, A. G., Boyes, A. F., Campbell, H. J., Cooper, R. A., Crampton, J. S., et al. (2015). New Zealand geological timescale NZGT 2015/1. *New Zealand Journal of Geology and Geophysics*, *58*(4), 398–403. https://doi.org/10.1080/00288306.2015.1086391

Ramsay, D. C., Herzer, R. H., & Barnes, P. M. (1997). *Continental shelf definition in the Lord Howe Rise and Norfolk Ridge regions: Law of the Sea Survey 177, Part 1—Preliminary results*. Australian Geological Survey Organisation Record 1997/54.

Recy, J., & Dupont, J. (1982). *Le sud-ouest du Pacifique: Données structurales carte à 1 : 12000000 à l'équateur. ORSTOM Notice Explicative* (Vol. 97). Office de la Recherche Scientifique et Technique Outre-Mer (ORSTOM).

Richer de Forges, B., & Chevillon, C. (1996). Les campagnes d'échantillonnage du benthos bathyal en Nouvelle- Calédonie, en 1993 et 1994 (BATHUS 1 à 4, SMIB 8 et HALIPRO 1). In A. Crosnier (Ed.), *Résultats des campagnes MUSORSTOM* (Vol. 15, pp. 33–53). Mémoire du Musée Nationale Histoires Naturelle.

Rickard, M. J., & Williams, I. S. (2013). No zircon U-Pb evidence for a Precambrian component in the Late Eocene Yavuna trondhjemite, Fiji. *Australian Journal of Earth Sciences*, *60*(4), 521–525. https://doi.org/10.1080/08120099.2013.792295

Rodda, P. (1994). Geology of Fiji. In A. J. Stevenson, R. H. Herzer, & P. F. Ballance (Eds.), *Geology and submarine resources of the Tonga-Lau-Fiji region*, SOPAC Technical Bulletin (Vol. 8, pp. 131–151).

Schaen, A. J., Jicha1, B. R., Hodges, K. V., Vermeesch, P., Stelten, M. E., Merceret, C. M., et al. (2021). Interpreting and reporting ^{40}Ar/^{39}Ar geochronologic data. *Geological Society of America Bulletin*, *133*(3–4), 461–487. https://doi.org/10.1130/b35560.1

Schellart, W. P., Lister, G. S., & Toy, V. G. (2006). A Late Cretaceous and Cenozoic reconstruction of the Southwest Pacific region: Tectonics controlled by subduction and slab rollback processes. *Earth-Science Reviews*, *76*(3–4), 191–233. https://doi.org/10.1016/j.earscirev.2006.01.002

Sdrolias, M., Müller, R. D., & Gaina, C. (2003). Tectonic evolution of the southwest Pacific using constraints from backarc basins. *Geological Society of America Special Paper*, *372*, 343–359.

Sdrolias, M., Müller, R. D., Mauffret, A., & Bernardel, G. (2004). The enigmatic formation of the Norfolk Basin, SW Pacific: A plume influence on back-arc extension. *Geochemistry, Geophysics, Geosystems*, *5*(6), Q06005. https://doi.org/10.1029/2003GC000643

Seton, M., Mortimer, N., Williams, S., Quilty, P., Gans, P. B., Meffre, S., et al. (2016). Melanesian back-arc basin and arc development: Constraints from the eastern Coral Sea. *Gondwana Research*, *39*, 77–95. https://doi.org/10.1016/j.gr.2016.06.011

Sevin, B., Maurizot, P., Cluzel, D., Tournadour, E., Etienne, S., Folcher, N., et al. (2020). Post-obduction evolution of New Caledonia. *Geological Society, London, Memoir*, *51*(1), 147–188. https://doi.org/10.1144/m51-2018-74

Shane, P., Strachan, L. J., & Smith, I. E. M. (2010). Redefining the Waitemata Basin, New Zealand: A new tectonic, magmatic, and basin evolution model at a subduction terminus in the SW Pacific. *Geochemistry, Geophysics, Geosystems*, *11*(4), Q04008. https://doi.org/10.1029/2009GC002705

Shervais, J. W. (2022). The petrogenesis of modern and ophiolitic lavas reconsidered: Ti-V and Nb-Th. *Geoscience Frontiers*, *13*(2), 101319. https://doi.org/10.1016/j.gsf.2021.101319

Stern, R. J. (2006). The anatomy and ontogeny of modern intra-oceanic arc systems. *Geological Society, London, Special Publication*, *338*(1), 7–34. https://doi.org/10.1144/sp338.2

Stern, R. J., Fouch, M. J., & Klemperer, S. L. (2003). An overview of the Izu-Bonin-Mariana Subduction Factory. *Geophysical Monograph*, *138*, 175–222.

Stratford, J. (2009). Mineralisation epochs within the Fiji Platform and their relationship to crustal development. *SOPAC Technical Bulletin*, *11*, 121–132.

Stratford, W. R., Sutherland, R., Dickens, G. R., Blum, P., Collot, J., Gurnis, M., et al. (2022). Timing of Eocene compressional plate failure during subduction initiation, northern Zealandia, southwestern Pacific. *Geophysical Journal International*, *229*, 1567–1585. https://doi.org/10.1093/gji/ggac016

Streckeisen, A., & Le Maitre, R. W. (1979). A chemical approximation to the modal QAPF classification of the igneous rocks. *Neues Jahrbuch fur Mineralogie Abhandlungen*, *136*, 169–206.

Strong, D. T., Turnbull, R. E., Haubrock, S. E., & Mortimer, N. (2016). Petlab: New Zealand's national rock catalogue and geoanalytical database. *New Zealand Journal of Geology and Geophysics*, *59*(3), 475–481. https://doi.org/10.1080/00288306.2016.1157086

Sutherland, R., Collot, J., Bache, F., Henrys, S., Barker, D., Browne, G. H., et al. (2017). Widespread compression associated with Eocene Tonga-Kermadec subduction initiation. *Geology*, *45*(4), 355–358. https://doi.org/10.1130/g38617.1

Sutherland, R., Dickens, G. R., Blum, P., Agnini, C., Alegret, L., Asatryan, G., et al. (2019). Expedition 371 summary. *Proceedings of the International Ocean Discovery Program*, *371*. https://doi.org/10.14379/iodp.proc.371.101.2019

Sutherland, R., Dickens, G. R., Blum, P., Agnini, C., Alegret, L., Asatryan, G., et al. (2020). Continental-scale geographic change across Zealandia during Paleogene subduction initiation. *Geology*, *48*(5), 419–424. https://doi.org/10.1130/g47008.1

Taylor, B., & Karner, G. D. (1983). On the evolution of marginal basins. *Reviews of Geophysics*, *21*(8), 1727–1741. https://doi.org/10.1029/rg021i008p01727

Timm, C., de Ronde, C. E. J., Hoernle, K., Cousens, B., Wartho, J.-A., Caratori Tontini, F., et al. (2019). New age and geochemical data from the southern Colville and Kermadec Ridges, SW Pacific: Insights into the recent geological history and petrogenesis of the Proto-Kermadec (Vitiaz) Arc. *Gondwana Research*, *72*, 169–193. https://doi.org/10.1016/j.gr.2019.02.008

Todd, E., Gill, J. B., & Pearce, J. A. (2010). A variably enriched mantle wedge and contrasting melt types during arc stages following subduction initiation in Fiji and Tonga, southwest Pacific. *Earth and Planetary Science Letters*, *335–336*, 180–194. https://doi.org/10.1016/j.epsl.2012.05.006

Turner, G. (1971). Argon 40-argon 39 dating: The optimisation of irradiation parameters. *Earth and Planetary Science Letters*, *10*(2), 227–234. https://doi.org/10.1016/0012-821x(71)90010-0

van de Lagemaat, S. H. A., Mering, J. A., & Kamp, P. J. J. (2022). Geochemistry of syntectonic carbonate veins within Late Cretaceous turbidites, Hikurangi Margin (New Zealand): Implications for a mid-Oligocene age of subduction initiation. *Geochemistry, Geophysics, Geosystems*, *23*(5), e2021GC010125. https://doi.org/10.1029/2021GC010125

Watts, A. B., Weissel, J. K., & Davey, F. J. (1977). Tectonic evolution of the South Fiji marginal basin. In M. Talwani & W. C. PitmanIII (Eds.), *Island Arcs Deep Sea Trenches and Back Arc Basins* (Vol. 1, pp. 419–427). American Geophysical Union Maurice Ewing Series.

Whattam, S. A. (2009). Arc-continent collisional orogenesis in the SW Pacific and the nature, source and correlation of emplaced ophiolitic nappe components. *Lithos*, *113*(1–2), 88–114. https://doi.org/10.1016/j.lithos.2008.11.009

Whattam, S. A., Malpas, J., Ali, J. R., & Smith, I. E. M. (2008). New SW Pacific tectonic model: Cyclical intraoceanic magmatic arc construction and near-coeval emplacement along the Australia-Pacific margin in the Cenozoic. *Geochemistry, Geophysics, Geosystems*, *9*(3), Q03021. https://doi.org/10.1029/2007GC001710

References From the Supporting Information

Banner, F. T., & Blow, W. H. (1965). Progress in the planktonic foraminiferal biostratigraphy of the Neogene. *Nature*, *208*, 1164–1166.

Black, L. P., Kamo, S. L., Allen, C. M., Davis, D. W., Aleinikoff, J. N., Valley, J. W., et al. (2004). Improved ^{206}Pb/^{238}U microprobe geochronology by the monitoring of a trace-element-related matrix effect; SHRIMP, ID-TIMS, ELA-ICP-MS and oxygen isotope documentation for a series of zircon standards. *Chemical Geology*, *205*(1–2), 115–140. https://doi.org/10.1016/j.chemgeo.2004.01.003

Black, L. P., Kamo, S. L., Williams, I. S., Mundil, R., Davis, D. W., Korsch, R. J., & Foudoulis, C. (2003). The application of SHRIMP to Phanerozoic geochronology: A critical appraisal of four zircon standards. *Chemical Geology*, *200*(1–2), 171188–188. https://doi.org/10.1016/s0009-2541(03)00166-9

Blow, W. H. (1969). Late Middle Eocene to Recent planktonic foraminiferal biostratigraphy. In P. Bronniman & H. H. Renz (Eds.), *Proceedings of the 1st International Conference on Planktonic Microfossils* (Vol. 1, pp. 199–241). EJ Bull.

Dalrymple, G. B., & Duffield, W. A. (1988). High precision ^{40}Ar/^{39}Ar dating of Oligocene rhyolites from the Mogollon-Datil volcanic field using a continuous laser system. *Geophysical Research Letters*, *15*(5), 463–466. https://doi.org/10.1029/gl015i005p00463

Ludwig, K. (2003). *Isoplot 3.00* (Vol. 4). Berkeley Geochronology Centre Special Publication.

Paton, C., Hellstrom, J., Paul, B., Woodhead, J., & Hergt, J. (2011). Iolite: Freeware for the visualisation and processing of mass spectrometric data. *Journal of Analytical Atomic Spectrometry*, *26*(12), 2508–2518. https://doi.org/10.1039/c1ja10172b

Pearce, N. J. G., Perkins, W. T., Westgate, J. A., Gorton, M. P., Jackson, S. E., Neal, C. R., & Chenery, S. P. (1997). A compilation of new and published major and trace element data for NIST SRM 610 and NIST SRM 612 glass reference materials. *Geostandards Newsletter*, *21*(1), 115–144. https://doi.org/10.1111/j.1751-908x.1997.tb00538.x

Spell, T. L., & McDougall, I. (2003). Characterization and calibration of ^{40}Ar/^{39}Ar dating standards. *Chemical Geology*, *198*(3–4), 189–211. https://doi.org/10.1016/s0009-2541(03)00005-6